**Diploma Thesis**

# EFFICIENT FINITE ELEMENT MODELLING OF RESIDUAL STRESSES IN MUTLILAYER COATINGS

carried out for the purpose of obtaining the degree of Master of Science (MSc or Dipl.-Ing), submitted at TU Wien,
Faculty of Mechanical and Industrial Engineering, by

**Antonia WAGNER**

1127267
Sechshauser Straße 28
1150 Vienna

under the supervision of
Ao. Univ. Prof. Dipl.-Ing. Dr. techn. Helmut Böhm
Assistant Prof. Dipl.-Ing. Dr. techn. Melanie Todt
Institute of Lightweight Design and Structural Biomechanics

reviewed by

Helmut Böhm
ILSB, E317

Paul Heinz Mayrhofer
WT, E308

Affidavit

I declare in lieu of oath, that I wrote this thesis and performed the associated research myself, using only literature cited in this volume. If text passages from sources are used literally, they are marked as such.

I confirm that this work is original and has not been submitted elsewhere for any examination, nor it is currently under consideration for a thesis elsewhere.

Vienna, June, 2017

Signature

## *Danksagung*

*An dieser Stelle möchte ich mich bei jenen Menschen bedanken, welche mich auf meinem Weg bis zum Ende dieses Studiums unterstützt haben. Besonderer Dank gilt meinen Betreuern Ao. Univ. Prof. Dipl.-Ing. Dr. techn. Helmut Böhm und Assistant Prof. Dipl.-Ing. Dr. techn. Melanie Todt für die hervorragend Betreuung. Die zahlreichen Gespräche waren stets sehr hilfreich und interessant. Weiters möchte ich mich bei meiner Familie bedanken, im Besonderen bei meinen Eltern, welche mir das Studium in dieser Form ermöglicht haben. Ein großes Dankeschön gebührt auch meinen Studienkollegen, wobei ich Andi, Schurli, Feili, Wurmsdi, Schachl und Höfler speziell dafür danken möchte, dass mit ihnen auch die stressigen Phasen des Studiums Zeiten waren, die ich nicht missen möchte. Weiters gilt mein besonderer Dank Pauli für sein Verständnis und seine Unterstützung während der gesamten Dauer meines Studiums.*

# Contents

# Abstract

The aim of this thesis is the development of an efficient finite element model to simulate multilayer systems comprising several hundred layers. These layers, each being a few nanometers thick, are deposited onto a substrate material by physical vapor deposition processes. After the manufacturing process residual stresses in the coating as well as in the substrate can be observed. Reaching a value of several GPa, the residual stresses lead to deformations and can result in damage or failure of the multilayer system. The stresses are induced primarily by two effects. Stresses originating from the film growth process contribute to the overall residual stress state. Furthermore, thermal stresses arise when cooling down the multilayer system from manufacturing conditions.

The finite element model should enable to determine the influence of process parameters on the residual stress state in the individual layers and the substrate.

A three dimensional model was developed and typical process conditions were applied. Special emphasis was laid on the computational efficiency of the simulation. This was achieved by modelling the individual layers with shell elements in conjunction with cohesive zone elements. Furthermore an infinite plate was modelled by applying periodic boundary conditions. This approach is reasonable due to the large ratio of lateral dimensions to thickness. Using this model, the influence of parameters, like layer and substrate material, on the residual stress state can be analysed.

In order to further consider the effect of a free edge on, the boundary conditions were modified and the influence on the interface stress state was investigated.

# Kurzfassung

Ziel dieser Arbeit ist die Erstellung eines effizienten Finite-Elemente-Modells zur Simulation von Multilayer-Beschichtungen bestehend aus einigen hundert Einzelschichten mit Dicken im Nanometer-Bereich. Diese Beschichtungen werden mithilfe von Verfahren der phsyikalischen Dampfphasenabscheidung auf ein Substratmaterial aufgebracht. Beim Fertigungsprozess entstehen Eigenspannungen sowohl in der Beschichtung als auch im Substratmaterial. Erreichen diese eine Größenordnung von einigen GPa, kommt es zu Deformationen, welche Schädigung oder Versagen des Materials zur Folge haben können. Die Eigenspannungen sind einerseits bedingt durch den Schichtwachstumsprozess, andererseits entstehen thermische Spannungen beim Abkühlen des Materials von der Fertigungs- auf Raumtemperatur.
Das Finite Elemente Modell soll dazu dienen, den Einfluss der Fertigungsprozessparameter auf den Spannungszustand der Schichten und des Substrats zu bestimmen. Ein dreidimensionales Modell wurde erstellt und für das Fertigungsverfahren typische Bedingungen wurden eingebracht. Besonderes Augenmerk wurde auf die Recheneffizienz der Simulation gelegt. Erreicht wurde diese durch den Einsatz von Schalenelementen zur Modellierung der einzelnen Schichten, welche mittels Kohäsivzonenelementen gekoppelt wurden. Weiters wurde zur Recheneffizienzsteigerung mithilfe von periodischen Randbedingungen eine unendlich große Platte modelliert. Dies ist aufgrund der Größe des Verhältnisses zwischen Bauteildicke und der lateralen Ausdehnung eine gute Näherung. An diesem Modell wurden die fertigungsbedingten Eigenspannungen in Abhängigkeit einiger Parameter, wie Beschichtungs- und Substratmaterial, analysiert. Um den Einfluss eines freien Randes mitzuberücksichtigen, wurden die Randbedingungen modifiziert und die Auswirkungen auf den Spannungszustand im Interface untersucht.

# Chapter 1

# Introduction

## 1.1 Nanoscale Multilayer Coatings

In the past decades interest in improving materials performance and efficiency for industrial purposes by surface engineering has increased. Especially thin film coatings technology has powered a constantly growing industry. Thin coatings are nowadays instrumental in a large number of fields of engineering and are utilised in a variety of applications such as optical coatings, semiconductor devices, optoelectronics and wear resistant coatings. By coating a substrate with a thin film, most commonly metal nitrides like TiN or CrN, a structure with improved mechanical properties, e.g. strength and toughness, can be obtained. When applying multiple layers composed of two or more alternating coating materials, the properties of the individual layer materials can be combined. The architecture of the multilayer can be periodic, have a set pattern or can be entirely random. Going one step further and reducing the thickness of the individual layers up to a few nanometers, so-called superlattice coatings can be obtained. These coatings exhibit properties different to the individual layer materials. The favoured properties can be tailored by varying the material and the thickness of the individual layers. Doing so, the multilayered coatings can show an improved performance with regard to hardness and fracture toughness com-

pared to a monolayer. For example, multilayer TiAlN/CrN coatings compared to a TiAlN monolayer exhibit higher hardness and elastic modulus and smaller grain size [7, 11, 18, 31].

By using physical vapor deposition (PVD), employing either evaporation or sputtering for the coating deposition, the desired structure of multiple nanolayers can be attained [26]. However, manufacturing results in residual stresses in the coating and the substrate that may reach a magnitude sufficient for inducing mechanical deformation, damage or failure of the multilayer system. These residual stresses have two primary origins. The evolutionary nature of the film microstructure and structural defects induced during the film growth process result in compressive stresses in the coating. Furthermore, due to the elevated manufacturing temperature, the mismatch of the thermal expansion coefficients of the substrate and the individual layers forming the coating leads to thermal residual stresses at room temperature. The consequent residual stresses play an important role in the range of performance of the material since they influence the mechanical integrity of the coating [28].

## 1.2 State of the Art

A brief overview of research related to the present study is presented in this Section. Both, analytical and numerical approaches to investigating the residual stress distribution in multilayer systems remote from free edges and their combination with experimental results are treated. Furthermore, representative examples of published approaches for the investigation of the stress distribution in the vicinity of a free edge are reviewed.

An analytical approach to estimating the relation between the specimen curvature and the residual stresses in thin films was first formulated by Stoney [25]. Stoney's formula involves several assumptions. Among other restrictions, only homogeneous, isotropic and linear elastic material behaviour can be considered and the radius of curvature must be equal in both in-plane directions.

Tsui et al.[30] developed an analytical model to predict the residual stresses in progressively deposited coatings due to thermal and intrinsic stresses using force and momentum equilibria. With this model the relative contributions of the two stress generation mechanisms to the final residual stress state were determined.

A finite element model to determine the residual stresses due to thermal expansion mismatch in a system consisting of a substrate and two layers was developed in [14]. The geometry was simplified by a cylindrical model using 2D elements and cooling from manufacturing to room temperature was simulated. The results were compared with an analytical model and experimental data obtained with X-ray diffraction technique.

Zhu et al.[34] applied three-dimensional digital image correlation to evaluate the curvature of a specimen and implemented the experimental result in a 2D finite element simulation using plane stress elements. The curvature was measured after the coating process at manufacturing temperature and at room temperature. The first value, which results from the intrinsic stresses, is implemented in the FE-simulation as an "imaginary" temperature change leading to compressive stresses, the second curvature value results from the thermal stresses. An ideal elastic-plastic model with von Mises yield criterion was adopted for the substrate and the bonded layer.

To determine a more realistic stress profile over the film thickness Massl et al.[16] presented a new approach, the so-called ion beam layer removal method (ILR). A bending experiment with a cantilever consisting of a substrate material and a thin film allows to determine the stress distribution. The layer is removed gradually and after each removal step the deflection is measured from scanning electron microscope (SEM) images. With the elastic properties of the coating and the cantilever dimensions, the stress profile is calculated analytically and plotted as a function of the total thickness.

In [23] the ILR method is used to determine the stress distribution of a multilayer system by means of an analytical calculation and a finite element simulation. In the FE-model each sublayer is modelled with one continuum element over the height to

save computation time. A comparison of the two approaches shows a good correlation when applying the same boundary conditions to the FE-model as considered in the analytical method based on the Euler-Bernoulli theory. However, the stress distribution in the layers cannot be resolved when modelled with only one continuum element.

In [32] the influence of the residual stresses on fracture and delamination in relation to the interface topography, coating thickness and elastic mismatch was investigated for monolayer coatings. A finite element model was created, characteristic residual stresses were applied and the effects on the interfacial region were analysed.

Yu et al.[33] considered a monolayer film under uniform tension and investigated analytically the free edge effect on the residual stresses on a two-dimensional plane strain configuration with an existing crack. The presented approach is not very accurate for short cracks and must be modified for the consideration of compressive residual stresses.

An instructive example for understanding the stress state in a bilayer compound was presented in [1]. The two layers are assumed to have same dimensions and elastic properties. For this simple case the analytical solutions are compared with finite element results obtained for two different situations assuming either plane stress or plane strain.

It can be summarized that analytical approaches require many assumptions, such as homogeneous and isotropic material, whereas finite element simulations are mostly modelled in 2 dimensions or without a proper discretization of the thin layers when using continuum elements to save computational calculation time.

## 1.3 Motivation

Despite the fact that residual stresses in coatings have been investigated extensively, there are many possibilities for improvement regarding the efficiency of the underlying computational models and the reliability of the analytical calculations. Analytical approaches are mostly restricted to 1-dimensional problems with linear elastic material behaviour and cannot provide information about the stresses in the interfaces between the substrate and the layers. Numerical approaches encounter their limits when it comes to the simulation of a high number of layers leading to excessive calculation times.

The aim of the present study is to improve the computational efficiency of finite element models of multilayer systems without a loss of accuracy. The model should enable simulating coatings with several hundred individual layers, each being just a few nanometers thick. In order to achieve this, the element types and boundary conditions applied to the model have to be chosen in a reasonable manner. In particular, applying periodic boundary conditions and using shell elements for modelling the individual layers are the two main measures aiming to decrease the computational effort.

Within this framework the residual stress state in the substrate and the individual layers due to the deposition process is to be examined. By changing the magnitude of the loads in the FE analysis input, a variation of the process parameters can be simulated. Furthermore, considering an infinite plate model, the influence of the dimensions and materials of the multilayer system on the residual stress state is to be investigated. Another model is to be developed which enables to consider the influence of a free edge on the stress magnitude and distribution in the interface and potential damage. Accurate predictions of the residual stresses in multilayer coatings obtained from the FEM model will be used to provide initial configurations for further simulations and can consequently improve the final results.

# Chapter 2

# Theoretical Background

## 2.1 Manufacturing Process of Multilayer Coatings

The variety of production methods of thin films is vast, the two main processes being chemical vapor deposition (CVD) and physical vapor deposition (PVD).
In the following sections the PVD technique, especially the sputtering and arc evaporation processes, will be discussed in detail, since these are the methods used for the manufacturing of coatings investigated in this study.

### 2.1.1 Physical vapor deposition

Physical vapor deposition generally describes any process depositing thin films by the condensation of a vaporized form of a solid material. The three major methods are evaporation, sputtering and ion plating, each comprising different variants [3].
A substantial advantage of PVD methods compared to other processes is the simple variation of coating properties. This can be achieved by adjusting the process parameters like substrate temperature, deposition rate, degree of ionisation etc. Furthermore, virtually any coating material can be deposited on a great variety of substrate materials [13].

Each deposition process can be divided into three basic steps. First of all the solid coating material is converted into its vapor phase. The second task is to transport the vapor species from the source to the substrate. The third step includes the condensation of vapors which then nucleate and grow on the substrate [3].
To obtain a vapor by a purely physical process, the source material (target) is either evaporated by heating or by bombardment with ions, referred to as sputtering. In order to achieve an essentially line-of-sight transport of the vaporized atoms prior to the condensation on the substrate, sputtering and evaporation processes are commonly carried out in vacuum [3, 18].

### Sputtering process

The technique of sputtering is based on bombardment of the coating material, referred to as the target, with positive gas ions, resulting in a vapor.
These ions, usually from an inert gas like Argon, are obtained by applying a negative voltage to the target which results in an electrical gas discharge. The electrons then collide with the inert gas atoms causing their ionization. The positive ions are attracted to the negatively charged target, i.e. the cathode. As a result the ions accelerate and strike the target. A momentum transfer from the Argon ions to the surfafe atoms of the target results in their ejection, referred to as sputtering. The sputtered atoms condense on the substrate and form a thin film. If the electron trajectories are only defined by the electrical field between the anode, where the substrate is attached to, and the cathode, the rapid loss of electrons is a problem. In order to trap the electrons, a magnetic field is applied. The probability of ionizing increases and hence the discharge pressure can be reduced. This results in an increased film quality [3, 18]. A schematic diagram of unbalanced magnetron sputtering with three metals, Cr, Al and Zr, as targets is shown in Fig. 2.1.

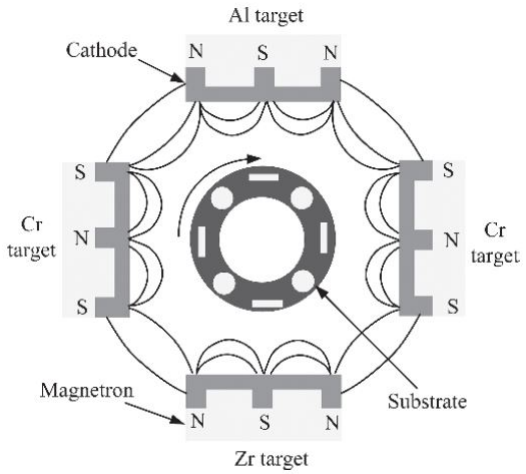


**Figure 2.1:** Schematic diagram of unbalanced magnetron sputtering [15]

### Arc Evaporation process

In contrast to the sputter deposition, the arc evaporation is a thermal vaporization process and no working gas is necessary. A high current, low voltage arc is used to vaporize a cathodic electrode, i.e. the target, giving rise to a small, highly energetic emitting area, referred to as the arc spot. Due to the extremely high temperature at the arc spot, resulting in a high velocity jet of vaporized material, a crater is left behind on the target surface. The randomly moving arc can be steered by magnetic fields in order to use the entire surface. The delivered energy in this process is high enough to allow ionization of the evaporated material. To accelerate the ions towards the substrate surface, the substrate is biased. Then the ionized material condenses on the substrate material.
Arc evaporation is mainly used for hard and decorative coatings [17].

## 2.2 Origins of Residual Stresses

After the manufacturing process of thin coatings, the substrate and the individual layers are stressed without applying any external forces $F_i$ or moments $M_i$, repre-

sented by the following formulas

$$\sum_{i=1}^{n} F_i = \sum_{i=1}^{n} \int_{h_{i-1}}^{h_i} \sigma_i(z)\, \mathrm{d}A_i = 0 \tag{2.1}$$

$$\sum_{i=1}^{n} M_i = \sum_{i=1}^{n} \int_{h_{i-1}}^{h_i} \sigma_i(z)\, z \mathrm{d}A_i = 0 \tag{2.2}$$

with $\sigma_i$ being the stress distribution in each component $i$, i.e. the substrate with $i$=1 and the individual layers, as a function of $z$ and $A_i$ being the integration area.
The residual stresses $\sigma(z)$ in thin coatings are usually divided into two categories, the extrinsic and the intrinsic stresses, $\sigma_{\mathrm{ext}}$ and $\sigma_{\mathrm{int}}$, respectively. The intrinsic stresses are primarily caused by film growth, the extrinsic stresses include the thermal stresses $\sigma_{th}$ and the epitaxial stresses $\sigma_{\mathrm{epi}}$. The stresses caused by epitactic or structural misfit between the nucleated film and the substrate are assumed to be negligible, but could also be incorporated if necessary [21].

$$\sigma = \sigma_{\mathrm{int}} + \sigma_{\mathrm{th}} + \sigma_{\mathrm{epi}} \tag{2.3}$$

### 2.2.1 Film Growth

During the deposition of a coating material on a substrate an internal stress state is generated due to the evolutionary nature of the film microstructure passing several growth stages.
At first the atoms, referred to as adatoms, nucleate and form isolated islands when condensing on the substrate. These islands grow due to further deposition and finally coalesce with other islands, forming grain boundarys.
Deposition is generally a non-equilibrium process, which means that the coating atoms are not in a relaxed position when condensing on the substrate material, resulting in a stressed state of the layer. In Fig. 2.2 the average stress in a polycrystalline

monolayer as a function of the layer thickness can be observed. Such diagrams can be obtained by the measurement methods described in Section 2.3.

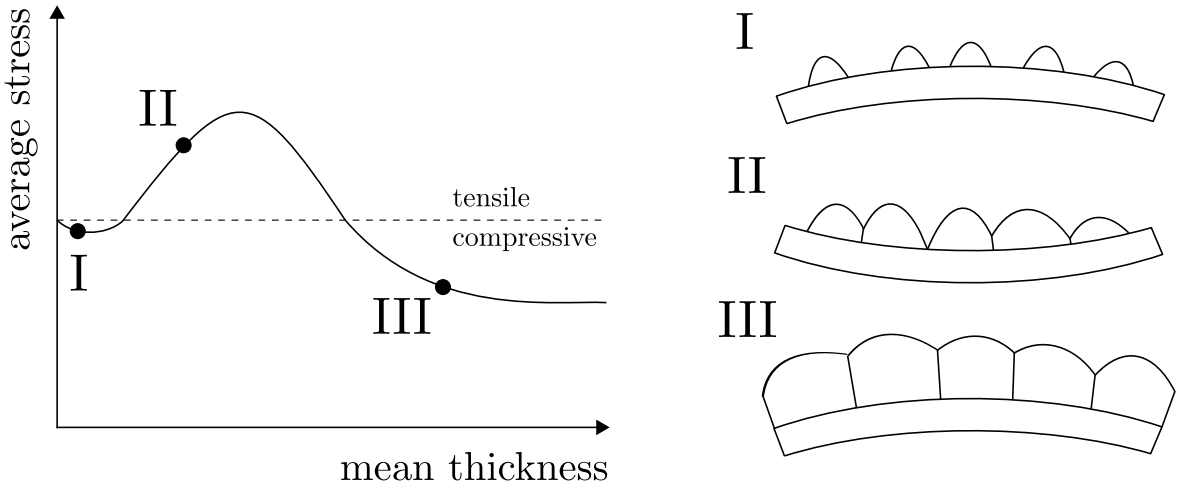


**Figure 2.2:** Schematic diagram of volume-average film stress versus mean film thickness (modified from [6])

**Pre-coalescence stress (I)**

Due to the initial compressive stress that is observed, it is assumed that the islands are more dense (have a smaller lattice parameter) than in an equilibrium state. The bonding between the island and the substrate has to be broken in order to enable the island to grow. The lattice parameter increases with an increasing size of the islands, approaching the lattice parameter of the bulk. At some point the energy required for breaking the bonding between the substrate and the island is too high. Hence, the islands cannot achieve the lattice parameter of the bulk and remain in a compressive condition. The origin of the stresses in this stage of film growth is not fully understood yet and alternatives to the described mechanism have been proposed [5, 6].

**Stresses induced by grain boundary formation (II)**

As indicated by the average stress versus mean film thickness diagram, tensile stresses are generated as the islands start to coalesce. It was proposed that in this stage of film growth the neighbouring islands form grain boundaries and hence reduce their surface energy. Since the islands need to overcome some distance to snap together, the strain energy needed must be less than the reduction of surface energy. The

resulting strain in the individual islands leads to a tensile average stress in the film. This is known as the Nix-Hoffman mechanism [5, 6].

**Stresses due to insertion of atoms at the grain boundaries (III)**

The tensile stress maximum indicates the end of the grain boundary formation, with its value being dependent on the grain boundary motion and voids between the grains. To obtain a compressive stress, there must be an excess number of atoms in the film. Under the condition of continuous deposition flux and existing grain boundaries a non-equilibrium state is maintained at the growth surface. The elevated chemical potential of the surface is not enough for a diffusion of the adatoms into the crystal as they would be ejected rapidly, but acts as a driving force for the atoms to migrate to the grain boundaries. An average compressive stress state results from incorporation of excess atoms in the grain boundaries. This effect decreases with increasing compressive stress leading to an asymptotic value [5, 6].

**Stresses in multilayered coating due to renucleation**

When applying several layers on a substrate, each layer shows a new tensile maximum, but no small compressive minimum of the type formed by the deposition of a coating directly on the substrate. This can be explained by the roughness of the previous layer that allows coalescence of the newly nucleated islands with the existing surface, preventing compressive stresses which arise before coalescence of the islands. This process is depicted in Fig. 2.3, where $A$ indicates the new island. Coalescence of the individually nucleated islands of the new layer amongst themselves generates tensile stresses by the Nix-Hoffman mechanism. This is followed by compressive stresses due to insertion of atoms at the grain boundaries. By varying the thicknesses of the individual layers in a multilayer coating, the average stress can be varied between wide limits (compressive to tensile) [24].

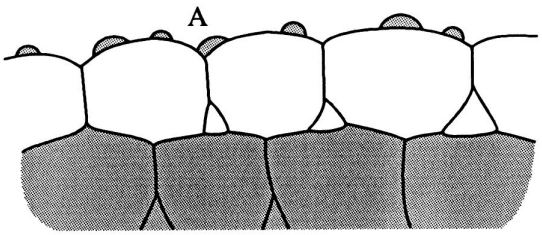


**Figure 2.3:** Renucleation at deposition of a new layer in a multilayer coating [24]

### Impact of process parameters on film growth

As already mentioned, deposition is generally a non-equilibrium process. Therefore, ambient conditions play an important role during the nucleation of the adatoms. In order to describe this influence, a variety of structure zone models (SZM) exists, defining the film morphology as a function of the deposition conditions. For evaporation processes, mainly the relation between the substrate temperature $T$ and the melting temperature of the deposited material $T_\mathrm{m}$ is the key factor for the morphology of the growing film. For sputtering two further parameters are of interest: the process pressure and incident ion energy. These parameters were first implemented in the SZM by Thornton[29] and Messier[19]. Fig. 2.4 shows the SZM of Thornton representing the influence of the homologous temperature $\frac{T}{T_\mathrm{m}}$ and the process pressure $p_\mathrm{A}$ on the film morphology. The various zones indicate differences in the structure of the film resulting from a change in surface mobility. The SZM helps in predicting the microstructure.

### Generation of stresses due to structural defects

Coatings deposited by processes which involve high kinetic energy, like sputtering and arc evaporation processes, show a higher compressive residual stress compared to other evaporation processes.

When growing a film with one of these methods, the bombardment of the substrate with the energetic ions causes different types of stress-inducing defects in the volume

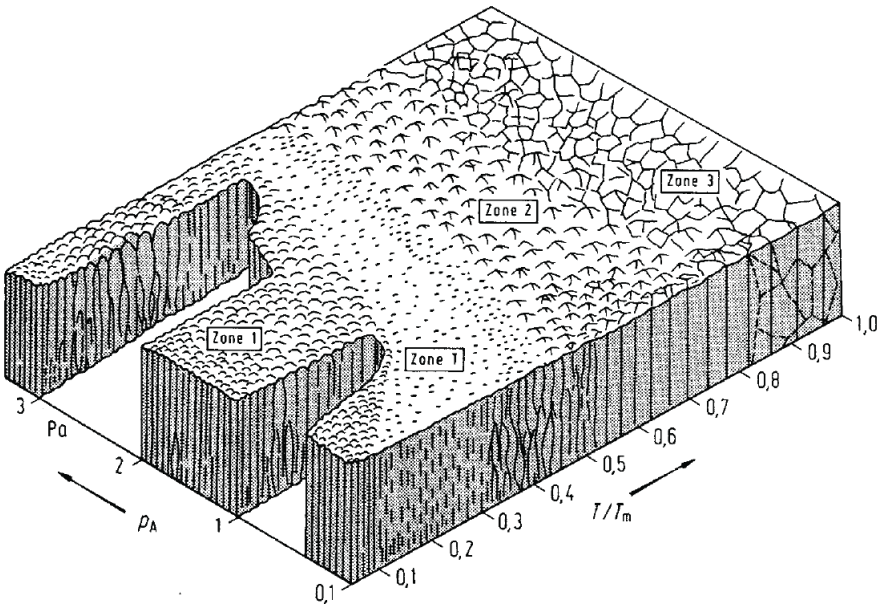


**Figure 2.4:** Structural zone model after Thornton [29]

of the grown layer, realized by, e.g., interstitial atoms or substitution of atoms. This process of stress modification is referred to as "atomic peening". The damage induced is dependent on several parameters like substrate temperature, gas pressure in the deposition chamber, degree of ionization etc. A low sputtering pressure causes less loss of energy due to collisions and the arriving atoms have higher energy. Hence lowering the pressure in the chamber at constant growth rate leads to films with a higher level of compressive stress. Unlike the effect of film growth rate in non-energetic processes, a higher growth rate in sputter deposition processes makes the film stress more compressive [5, 6, 21].

### 2.2.2 Thermal Expansion

When cooling down the multilayer system from its manufacturing conditions, the mismatch of the thermal expansion of the different materials results in residual stresses. The magnitude of thermal expansion of a material is defined by its coefficient of thermal expansion (CTE). It relates the material's change in linear dimensions to

a change of temperature. When the thermal expansion behaviour is nonlinear, as shown in Fig. 2.5, the CTE becomes temperature dependent. It can be specified either as an instantaneous or an total value.

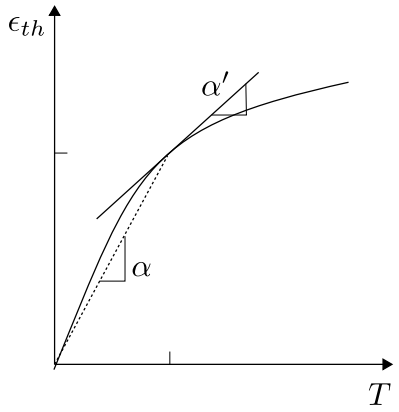


**Figure 2.5:** Definition of the instantaneous and total thermal expansion coefficient [27]

The instantaneous (or tangent) coefficient of thermal expansion is defined as

$$\alpha'(T) = \frac{d}{dT}\varepsilon_{\mathrm{th}}(T) \tag{2.4}$$

where $\varepsilon_{th}$ is the thermal strain and $T$ is the temperature.
The definition of the total (or secant) coefficient of thermal expansion relates the thermal strain to the total temperature change from a reference temperature $T_{\mathrm{ref}}$.

$$\alpha(T) = \frac{\varepsilon_{\mathrm{th}}(T)}{T - T_{\mathrm{ref}}} \tag{2.5}$$

To obtain the total CTE for a given temperature T, the instantaneous CTE has to be integrated using

$$\alpha(T) = \frac{1}{T - T_{\mathrm{ref}}} \int_{T_{\mathrm{ref}}}^{T} \alpha'(T)\,\mathrm{d}T \tag{2.6}$$

under consideration of the reference temperature.

### Generation of thermal residual stresses

When cooling down a multilayer system from its manufacturing conditions to room temperature, a bending moment is induced (see Fig. 2.6). This effect is attributed to the discrepancy between the coefficients of thermal expansion of the substrate and the coating material.

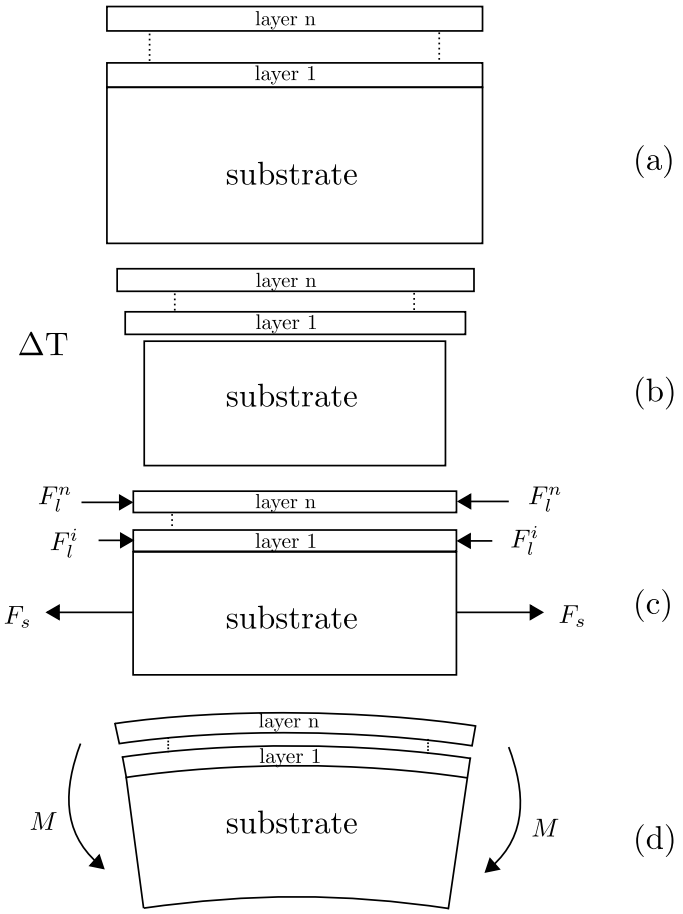


**Figure 2.6:** Generation of thermal residual stress in a multilayer coating

If we consider a temperature change $\Delta T$ of the individual materials, unconstrained strains are induced in the substrate and the coating, as shown in Fig. 2.6 (b). Due to the difference in thermal expansion coefficients, a misfit strain is created. For a

single layer on a substrate the thermal misfit strain is defined as

$$\Delta\varepsilon_{\mathrm{th}} = (\alpha_{\mathrm{C}} - \alpha_{\mathrm{S}}) * (T_{\mathrm{m}} - T) \tag{2.7}$$

where $\alpha_{\mathrm{C}}$ and $\alpha_{\mathrm{S}}$ are the thermal expansion coefficients of the coating and the substrate, respectively, and $T_{\mathrm{m}}$ is the manufacturing temperature, where thermal strains are zero.

At the interface between different constituents a displacement compatibility condition has to be satisfied, generating thermal stress, Fig. 2.6 (c). This results in a bending of the entire coating-substrate-system as indicated in Fig. 2.6 (d).

If we assume elastic isotropy, a substrate with infinite dimensions, no plastic deformation and a biaxial stress state, the one-dimensional approximation of the thermal coating stress in a single layer system can be calculated according to

$$\sigma_{\mathrm{th}}(T) = \frac{E_{\mathrm{C}}}{1 - \nu_{\mathrm{C}}}(\alpha_{\mathrm{C}} - \alpha_{\mathrm{S}}) * (T_{\mathrm{m}} - T) \tag{2.8}$$

where $E_{\mathrm{C}}$ is the Youngs modulus of the coating, $\nu$ the Poisson ratio of the layer. A negative value of $\sigma_{\mathrm{th}}$ indicates compressive stress. This is obtained if the substrate material shows a higher thermal expansion coefficient than the coating material, which is $\alpha_{\mathrm{S}} > \alpha_{\mathrm{C}}$, as indicated in Fig. 2.6. As a result of the present assumptions, the substrate is considered to be rigid without any strains in this approximation calculation.

## 2.3 Measurements of Residual Stresses

As stated before, the magnitude of thermal stresses can be estimated if the elastic and thermal material properties of substrate and coating are known, whereas for the intrinsic stresses no estimation is possible without experimental data.

In order to obtain the residual stress distribution in multilayer systems which are simulated in this study, either the stress state in the coating or the substrate curvature

can be measured. In the following the two most common methods for determining the average residual stress in thin films will be introduced.

### 2.3.1 X-ray Diffraction

X-ray diffraction relies on the interactions between the wave front of the X-ray beam and the crystal lattice. The normal lattice spacing $d$ can be determined by means of Bragg's law

$$d = \frac{n\lambda}{2\sin\theta} \tag{2.9}$$

where $\lambda$ is the wavelength of the beam, $\theta$ the scattering angle between the surface normal and the X-ray diffraction vector and $n$ is an integer.

When we consider an isotropic coating on a substrate material the state of strain in the coating alters the lattice spacing from the value in an unstressed crystal, Fig. 2.7. By measuring the diffraction angle $2\theta$, the lattice spacing can be estimated.

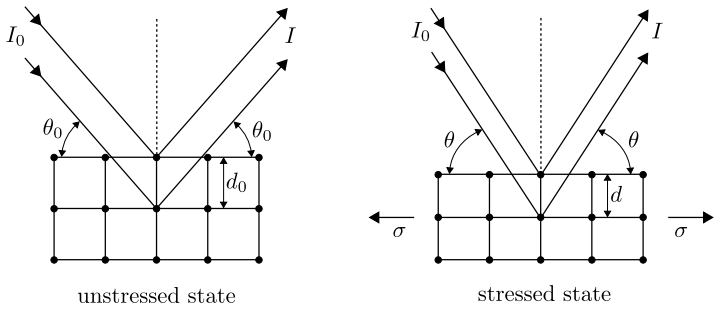


**Figure 2.7:** X-ray diffraction measurement: Change of lattice spacing due to elastic strain

The relation between the $d$ value and the strain normal to the plane of the coating is given as

$$\varepsilon(\theta) = \frac{d(\theta) - d_0}{d_0} \tag{2.10}$$

where $d_0$ is the strain free lattice spacing. In Fig. 2.8 $d$ is plotted as a function of $\sin^2(\psi)$, with $\psi$ being the angle between the surface normal and the direction of the strain being measured. The stress can be evaluated by calculating the slope

of the straight line and knowing the elastic properties of the material in the case of a rotationally symmetric stress state. Although the X-ray diffraction method is powerful in determining stress, it is not easy to monitor in-situ stress evolution [5, 6, 12].

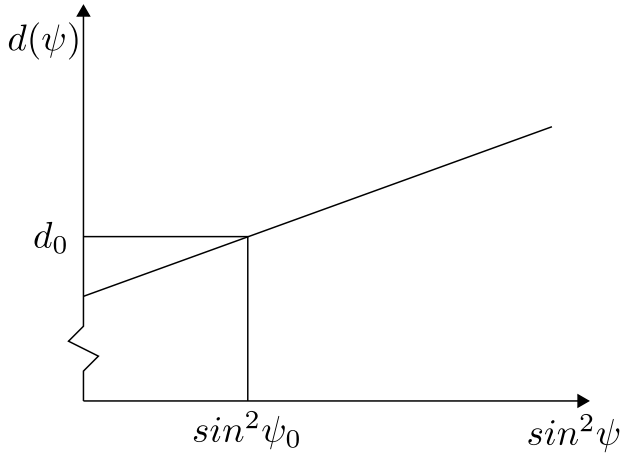


**Figure 2.8:** Schematic illustration of the determination of stress by X-ray diffraction method

### 2.3.2 Substrate Curvature Technique

As discussed in Section 2.2 stress in thin films induce a bending of the sample which results in a curvature $1/\rho \propto \varepsilon t$, with $\varepsilon$ being the average strain and $t$ the film thickness. With the substrate curvature technique either in-situ or ex-situ experiments can be carried out. Common methods for determining the curvature are the scanning laser method and the grid reflection technique. Fig. 2.9 shows the experimental setup with one laser beam. The laser beam incident on the sample is reflected by the surface and directed to a screen where the deflection is monitored. The thickness of the film $t$ can be determined by scanning electron microscopy (SEM). The variation of $1/\rho$ and $t$ is measured as a function of time during film growth or under external loads. Consequently the relation between layer thickness and average stress can be determined for linear elastic behaviour with an analytical or numerical approach [6, 12].

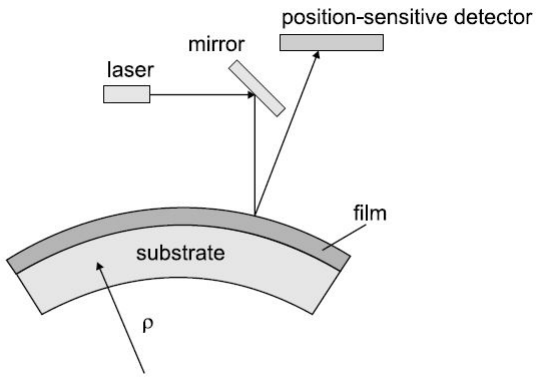


**Figure 2.9:** Sketch of a laser set-up for curvature measurement [6]

## 2.4 Influence of Residual Stresses on Mechanical Behaviour

The magnitude of residual stresses in films highly influences the performance of the substrate-coating systems, in terms of changing the thermo-mechanical behaviour or inducing damage. The residual stresses resulting from the manufacturing process are superposed on the stresses induced by external loads applied onto the system resulting in the total stress distribution. When the stress state in a multilayer coating exceeds certain limits, failure of the individual layers or the interfaces is induced in those regions. Especially internal defects or other geometrical variations, free edges, lead to stress concentrations, which can exceed the strength of the material. This may result in coating fracture and interfacial delamination [6].
The two dominant failure modes in the case of a compressive stress state of the coating are buckling-driven interface delamination and edge delamination. A typical failure mode due to high tensile stresses is cracking of the layers [2].

Within this framework the issue of interface delamination due to a free edge will be discussed. The residual stresses remote from a free edge are parallel to the interface for a planar geometry. In the vicinity of a free edge interfacial normal stresses, i.e.

parallel to the free surface at the edge, and shear stresses are induced locally. In this region the material is prone to mode I and II delamination [10].

# Chapter 3

# Finite Element Model

In this chapter the process of the generation of a finite element model for a nanoscale multilayer coating-substrate system is explained. Where necessary, brief descriptions of the theory concerning the finite element method is added.

In part of the present study a three dimensional finite representative unit cell is

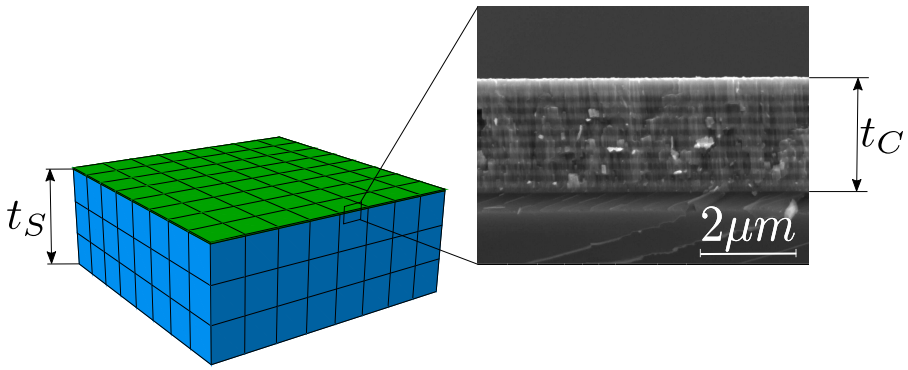


**Figure 3.1:** FEM-model and scanning electron microscopy image

modelled and two dimensional periodic boundary conditions are applied to examine the stress distribution in an infinite plate. For taking into account the effect of a free edge on the interface behaviour the geometry and the initially applied boundary conditions are modified.

In order to save computational time, the different constituents of the system, i.e. substrate, layers and interfaces, are modelled with different element families, reasonable for the individual requirements.
The origins of residual stresses explained in Section 2.2 are implemented in the analysis as two load cases which are finally combined. In this manner the effect of the manufacturing process on the residual stresses is represented and the variation of its process parameters is simulated.
Different modelling approaches for a multilayer coating of a total thickness $t_C$ deposited on a substrate of a thickness $t_S$, as shown in Fig. 3.1, are prepared: a homogenized coating, a composite shell section and layerwise modelling of the individual layers. A comparison of the results is discussed in the next chapter.
The numerical simulation of the multilayer system is realized using the FEM software package *Abaqus* [27]. The modelling strategies are formulated in a general way with reference to the *Abaqus*-specific designations.

## 3.1 Geometry and Mesh

The model of the multilayer system consists of the substrate, the layers and the interfaces between the substrate and the coating and between the individual layers of the coating. A three dimensional geometry of a representative unit cell is created using the finite element pre-processor *Hypermesh*. Generating the geometry and the mesh is parameter controlled and easily adjustable to different requirements. To achieve this adaptability a script generating the model in *Hypermesh* is set up with the programming language *Python*.
Within the script the substrate dimensions, the number of different layer materials, the layer architecture, the total number of layers, the thicknesses of the layers and the meshing can be set according to the requirements.
For the substrate a number of elements sufficient to resolve the stress distribution over the thickness is chosen. Regarding the in-plane dimensions a distinction must

be made between infinite plate models and models with a free edge.

**Infinite plate**

In the case of modelling an infinite plate, periodicity has to be applied in both in-plane directions $x$ and $y$, Fig. 3.2. Hence, no edge effects influence the results and the dimensions in this plane can be small. In the present study a quadratic hexahedral unit cell is modelled and the number of elements is chosen to make the resulting curvature of the model visible when using elements with linear interpolation.

**Semi-infinite plate**

For the semi-inifinite plate model, plane periodic boundary conditions are applied in only one of the in-plane directions. In the other direction symmetry conditions are applied on one side, the other face being left free to deform. To capture the stress distribution induced by the free edge effect, the dimension of the model in this direction has to be large enough to allow the stresses to decay. In the other in-plane direction the size can be small due to periodicity. Close to the free edge a mesh refinement is required.

Fig. 3.2 shows the meshes of the infinite plate model and the semi-infinite plate model.

## 3.2 Modelling Approach

The aim of the present study is simulating a nanoscale multilayer coating formed by up to several hundred bi-layers. An important factor for the computational efficiency of the numerical model is the choice of the element types. The simulation time depends primarily on the number of degrees of freedom (DOF) which define the number of equations that need to be solved during the analysis. The number of DOF in the overall system depends on the element families used, their order of interpolation, the number of DOF of each node and the modelling technique.

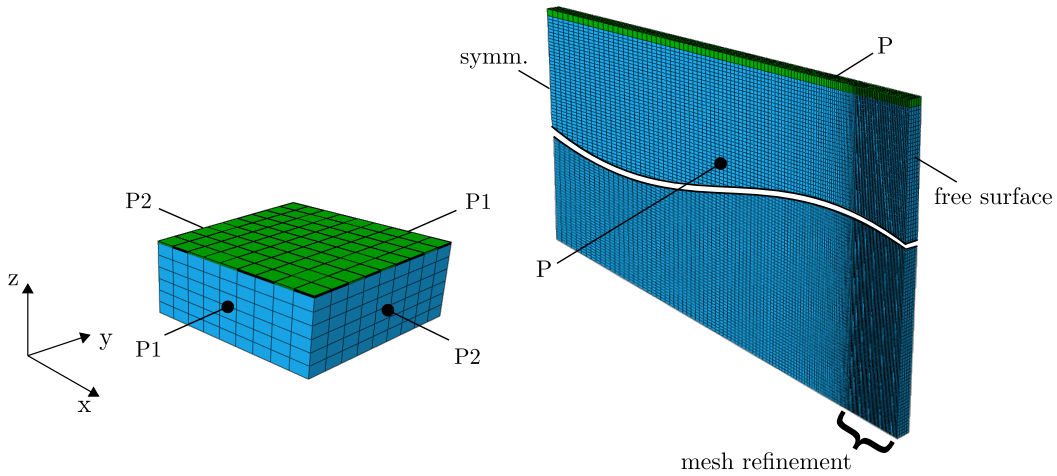


**Figure 3.2:** Meshes of the infinite plate model (left) and the semi-infinite plate model (right)

The type of elements used for the individual components substrate, layers and interfaces are set within the geometry and mesh generating script. The element types are chosen ensuring a compatible mesh. Furthermore no quadratic elements are considered for the substrate and layer modelling, since they are not compatible with the cohesive elements used within this study.

### 3.2.1 Substrate Modelling

The substrate material is modelled with 8-node three dimensional continuum elements with first-order interpolation and reduced integration (*Abaqus* element type: C3D8R). When using full integration, the elements can suffer from "shear locking", resulting in an overestimation of the stiffness. In order to avoid this error, elements with reduced integration can be used. Choosing these elements, however, can lead to difficulties solving the stiffness matrix and the effect of "hourglassing" can occur. For the present problem, modelling with reduced integration elements was found to be the appropriate approach. It is recommended that the elements dimensions do

not exceed an aspect ratio of 4 when modelling with continuum elements in order to ensure an acceptable element quality.

### 3.2.2 Layer Modelling

As mentioned before, the present model is intended to simulate a coating comprising several hundred layers each being very thin compared to the substrate. Hence, the computing effort for a single layer must be kept very small. By using continuum elements the stress distribution in the layer cannot be sufficiently well resolved when using one element over the thickness. If the discretization is chosen sufficiently fine in the thickness direction, also the mesh density in the in-plane direction must be raised in order to account for the element aspect ratio restrictions. To overcome this limitation, a shell-cohesive modelling approach is chosen, being computationally less demanding than continuum element modelling.

The use of shell elements is limited to structures that are very thin in one direction compared to the other dimensions. Using conventional shell elements a reference surface is defined to discretize a body and the thickness is defined by the section definition. Furthermore, zero stress is assumed in the shell thickness. In the case of continuum elements the entire three-dimensional body is modelled with the node coordinates defining the thickness. Another difference between the two element families is that continuum elements have three translational degrees of freedom per node, whereas shell elements have three rotational DOFs in addition.

Within this study 4-node conventional shell elements with linear interpolation and reduced integration (Type: *S4R*) are used. The shell thickness is defined in the section definition.

According to the default options in *Abaqus* the integration method in thickness direction is Simpson's rule with five integration points for a homogeneous shell section and three in each layer for a composite section.

For the stacking of the layers (discussed in Section 3.2.4) it is important to mention that the surface in the positive normal direction of the shell, defined by the node

numbering, is referred to as the positive face for contact definition. The surface in the negative direction along the normal is referred to as the negative face.
The reference plane of a shell element is the middle surface by default and can be changed by specifying an offset value [27].

### Layer modelling techniques

The modelling of the multilayer coating is realised by three different modelling approaches. For a first estimate of the stress distribution, the coating, which is actually deposited layer by layer, is modelled as a homogenized coating represented by one single layer. This method leads to a short simulation time but cannot capture the stress distribution in the individual layers and interfaces. Therefore it just provides an estimate of the stresses in the substrate, the interface between the substrate and the coating and the average stress value in the coating. It mainly serves for testing the modelling approach.
In order to increase the resolution of the stress distribution, the composite shell section definition is chosen as a second layer modelling technique. Within this option, one can define a single shell to be composed of layers made of different materials in different orientations. *Abaqus* determines the total thickness of the coating as the sum of layer thicknesses. Per default each layer contains three section points which enables to view the stress distribution in the individual layers. Nevertheless, the influence of (damage in) the interfaces between the layers cannot be captured.
Modelling the coating layerwise is most suitable for resolving the stress distribution in each layer including effects caused by the interface response. Furthermore, the magnitude of residual stress resulting from film growth can be varied for the different materials used in the coating. However, the number of DOF rises strongly resulting in a longer calculation time compared to the other two modelling methods.

### 3.2.3 Interface Modelling

The model developed within this thesis is aimed at being capable of investigating crack formation in the interfacial zone between the substrate and the coating or between the individual layers. To simulate crack initiation and propagation in numerical models several analysis techniques are available, including the virtual crack closure technique (VCCT) and Cohesive Zone Modelling [8].

In the present thesis the interface is modelled with cohesive zone elements. A relative motion of the top and bottom faces in thickness direction, as shown in Fig. 3.3, represents opening or closing of the interface. The transverse shear behaviour of the cohesive element is defined by the relative position change of these faces in the plane orthogonal to the thickness direction. It is assumed that stretching and in-plane shearing of the midsurface do not generate any stresses.

For three-dimensional simulations, the cohesive elements are formulated as 8-node three-dimensional elements (Type: *COH3D8*).

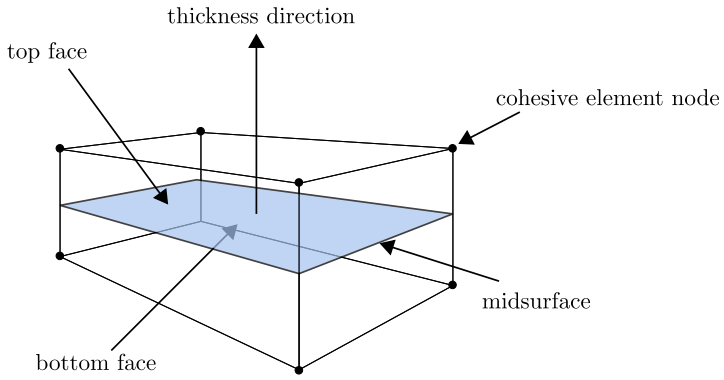


**Figure 3.3:** Spatial representation of a three-dimensional cohesive element (modified from [27])

#### Elastic traction-separation behaviour

If the thickness of the interface is negligibly small, like in the present model, the behaviour of the cohesive elements can be described using a traction-separation law (cohesive law). Doing so, *Abaqus* assumes a linear-elastic behaviour until damage

initiation, followed by damage evolution.

If we assume that a separation in normal direction does not generate cohesive stress in shear direction and vice versa, an uncoupled cohesive law is obtained. This elastic behaviour can be written in the following way:

$$\begin{Bmatrix} t_n \\ t_s \\ t_t \end{Bmatrix} = \begin{bmatrix} E_{nn} & 0 & 0 \\ 0 & E_{ss} & 0 \\ 0 & 0 & E_{tt} \end{bmatrix} \begin{Bmatrix} \varepsilon_n \\ \varepsilon_s \\ \varepsilon_t \end{Bmatrix} = \boldsymbol{E}\boldsymbol{\varepsilon} \tag{3.1}$$

with

$$\varepsilon_n = \frac{\delta_n}{T_0}, \varepsilon_s = \frac{\delta_s}{T_0}, \varepsilon_t = \frac{\delta_t}{T_0} \tag{3.2}$$

Within this equation the terms $t_n$, $t_s$, $t_t$ represent the components of the nominal traction stress vector in normal direction and the two shear directions. $\boldsymbol{E}$ represents the elastic stiffness, $\boldsymbol{\varepsilon}$ the vector of nominal strains, $\delta_n$,$\delta_s$ and $\delta_t$ the corresponding separations and $T_0$ the original thickness of the cohesive element [27].

In Fig. 3.4 a typical behaviour of the cohesive elements defined by a traction-separation law is illustrated.

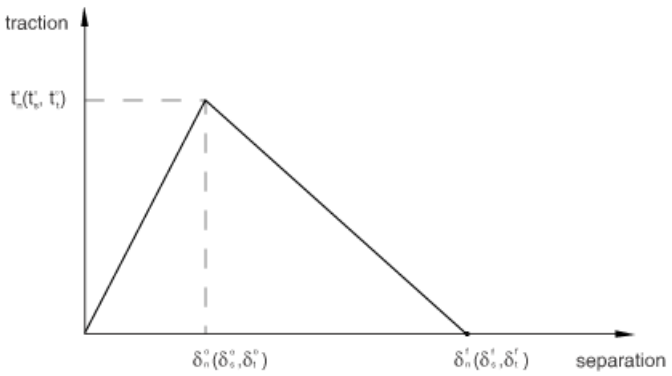


**Figure 3.4:** Linear traction-separation law [27]

### Damage initiation

The beginning of the degradation of the stiffness of the interface described with cohesive zone elements is defined by a damage initiation criterion. It either refers to a critical stress state or a critical strain. By using this criterion also the tendency of damage in the material can be defined without the need to specify the concrete damage evolution.

One possible damage initiation criterion is the so-called *Quadratic nominal stress criterion*. Damage is assumed to initiate when the following equation is satisfied:

$$\left\{\frac{\langle t_n \rangle}{t_n^0}\right\}^2 + \left\{\frac{t_s}{t_s^0}\right\}^2 + \left\{\frac{t_t}{t_t^0}\right\}^2 = 1 \tag{3.3}$$

where $t_n^0$, $t_s^0$, $t_t^0$ represent the maximum allowable nominal stresses for the case that the separation takes place purely normal to the interface or purely in the first or the second shear direction. The sharp brackets within the formula signify that a pure compressive stress does not initiate damage [27].

### Damage evolution

In order to describe the degradation of the material stiffness once the criterion for damage initiation is reached, a damage evolution law has to be defined. To do so, a scalar damage variable $D$ is introduced. By further loading after damage initiation $D$ evolves monotonically from 0 to 1. The nature of this evolution can be described either by a linear or exponential softening law between damage initiation and final failure.

To capture the cohesive zone traction distribution close to a free edge a mesh refinement is required.

### 3.2.4 Assembly

Due to the matching meshes, the cohesive elements can be connected to the continuum and shell elements simply by sharing the same nodes. The geometrical height of the cohesive elements is defined by the distance of the nodes. As the reference plane of the shell elements the mid-plane(*MID*) is defined. Doing so, the integration points of the cohesive zone model lie in between the two adjacent shell planes.

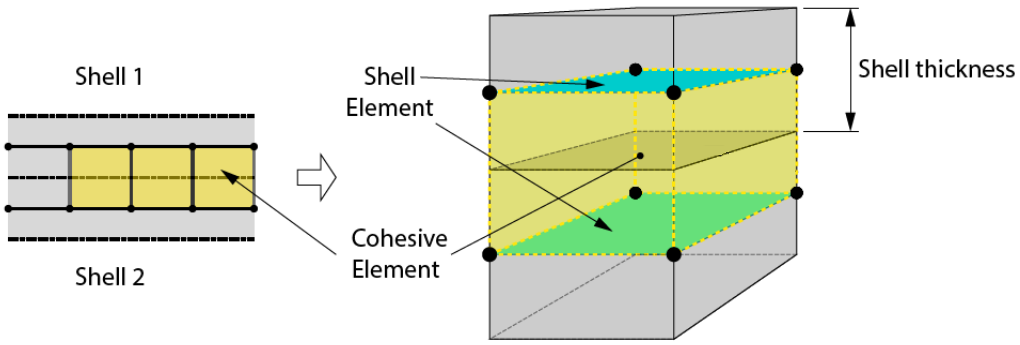


**Figure 3.5:** Assembly of a cohesive element with two shell elements [4]

## 3.3 Boundary Conditions

In this study a system with up to hundreds of layers and an overall thickness that is very small compared to the in-plane dimensions is considered. Modelling the entire geometry would lead to excessive simulation times. However, reducing the lateral dimensions and modelling just a small volume element may results in unrealistic stresses due to edge effects.

To overcome this limitation the multilayer-substrate-system is partitioned into periodically repeating unit cells. In this way an infinite plate can be simulated with reasonable computational effort. To simulate a semi-infinite plate with one free edge, the periodic boundary conditions have to be modified.

Periodic unit cells can be classified by the number of the axes of periodicity. In this thesis we have to consider the case of two axes of periodicity to model an infinite plate, referred to as plane periodic media. The model of the semi-infinite plate only uses one axis of periodicity and symmetry boundary conditions for one of the other axes. Periodic boundary conditions can further be classified according to the dimension of the model, being three in the present study. Fig. 3.6 shows schematic illustrations of the considered unit cell with the notation of the faces and corners. Within the definition of the periodic boundary conditions, the axes of the coordinate system are 1,2, and 3.

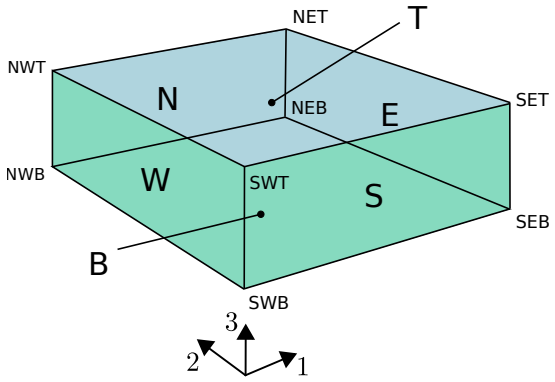


**Figure 3.6:** Entire unit cell with nodeset nomenclature

### 3.3.1 Applying PBC in Finite Element Analysis

In order to fulfil the condition that the strains on the lateral faces of the unit cell are compatible, i.e., neither separation nor overlapping occur, the displacement fields must be equal up to a rigid displacement for the opposite sides. The strain controlled periodic boundary conditions can not be directly applied as homogenized strains in the finite element model. Rather the displacements of characteristic nodes, referred to as *master nodes*, are specified.

The master nodes chosen for the plane periodic boundary conditions are the following: SWB, NWB, SEB, SWT. The displacement of the remaining corner nodes, referred

to as slave nodes, are related to the master node displacements. The displacements of the edge and face nodes are defined by the nodal displacements of the opposite edge/face and the master node displacements. For the sake of simplicity of the equations, the origin of the coordinate system lies in the corner SWB.

**Infinite plate**

For the case of two axes of periodicity the equations obtained for the translational degrees of freedom of the nodesets lying on the lateral faces have the following form [22]

$$\underline{u}^E - \underline{u}^W = \begin{pmatrix} u_1^{SEB} - u_1^{SWB} \\ u_2^{SEB} - u_2^{SWB} \\ u_3^{SEB} - u_3^{SWB} \end{pmatrix} + \begin{pmatrix} \frac{1}{l_3}\big((u_1^{SET} - u_1^{SEB}) - (u_1^{SWT} - u_1^{SWB})\big)x_3 \\ \frac{1}{l_3}\big((u_2^{SET} - u_2^{SEB}) - (u_2^{SWT} - u_2^{SWB})\big)x_3 \\ -\frac{1}{l_3}\big((u_2^{SET} - u_2^{SEB}) - (u_2^{SWT} - u_2^{SWB})\big)x_2 \end{pmatrix} \tag{3.4}$$

$$\underline{u}^N - \underline{u}^S = \begin{pmatrix} u_1^{NWB} - u_1^{SWB} \\ u_2^{NWB} - u_2^{SWB} \\ u_3^{NWB} - u_3^{SWB} \end{pmatrix} + \begin{pmatrix} \frac{1}{l_3}\big((u_1^{NWT} - u_1^{NWB}) - (u_1^{SWT} - u_1^{SWB})\big)x_3 \\ \frac{1}{l_3}\big((u_2^{NWT} - u_2^{NWB}) - (u_2^{SWT} - u_2^{SWB})\big)x_3 \\ -\frac{1}{l_3}\big((u_1^{NWT} - u_1^{NWB}) - (u_1^{SWT} - u_1^{SWB})\big)x_1 \end{pmatrix} \tag{3.5}$$

where $u_i^P$ is a nodal variable of the nodeset P for the degree of freedom i.

In the case of the multilayer coating model, the layers are modelled with shell elements, having additionally three rotational degrees of freedom, $\phi_i$ with $i$=1,2,3. Consequently the periodicity also has to be applied to the rotational degrees of freedom of the lateral faces of the unit cell. In Fig. 3.7 the nodesets comprising the lateral faces of the shell elements forming the multilayers are shown.

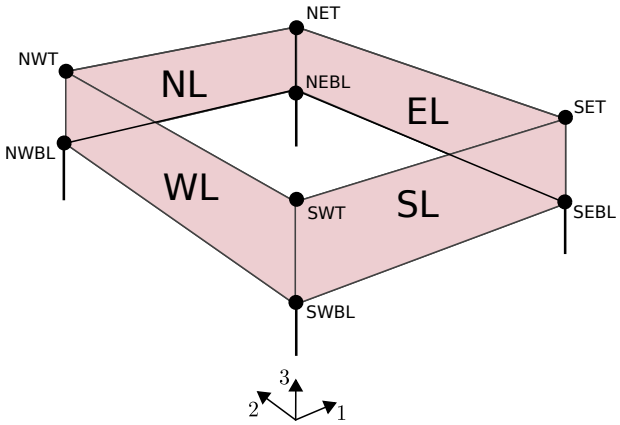


**Figure 3.7:** Part of the unit cell with nodeset nomenclature of the coating

The equations obtained for the rotational degrees of freedom in the case of two axes of periodicity can be written as:

$$\underline{\phi}^{EL} - \underline{\phi}^{WL} = \begin{pmatrix} -\frac{1}{l_3}\left((u_2^{SET} - u_2^{SEB}) - (u_2^{SWT} - u_2^{SWB})\right) \\ \frac{1}{l_3}\left((u_1^{SET} - u_1^{SEB}) - (u_1^{SWT} - u_1^{SWB})\right) \\ 0 \end{pmatrix} \tag{3.6}$$

$$\underline{\phi}^{NL} - \underline{\phi}^{SL} = \begin{pmatrix} -\frac{1}{l_3}\left((u_2^{NWT} - u_2^{NWB}) - (u_2^{SWT} - u_2^{SWB})\right) \\ \frac{1}{l_3}\left((u_1^{NWT} - u_1^{NWB}) - (u_1^{SWT} - u_1^{SWB})\right) \\ 0 \end{pmatrix} \tag{3.7}$$

In *Abaqus* the PBCs are applied through linear constraint equations. The relative motion of the nodes is defined by a linear combination of nodal variables which is equal to zero.

The boundary conditions applied additionally to the periodic boundary conditions to prevent rigid-body motion are given by:

$$u_1^{SWB} = u_2^{SWB} = u_3^{SWB} = 0 \tag{3.8}$$

$$u_1^{SWT} = u_2^{SWT} = 0 \tag{3.9}$$

$$u_1^{NWB} = 0 \tag{3.10}$$

$$u_2^{SEB} = 0 \tag{3.11}$$

The first line of Equ.(3.4) written in the form needed in the *Abaqus* input file and considering the additional boundary conditions reduces to the following equation

$$0 = -\underline{u}^E + \underline{u}^W + u_1^{SEB} + \frac{x_3}{l_3}(u_1^{SET} - u_1^{SEB}) \tag{3.12}$$

Fig. 3.8 shows a possible deformation state of the faces S, N, E, W and B in the case of an infinite plate model. The bearing symbols represent the additionally applied boundary conditions. If we consider the view in positive 2-direction, the face S is depicted.

It can be seen, that face W and E have the same deformation apart from a uniform displacement. The same applies to the faces N and S. As part of the lateral faces, also the edges of the bottom and top face(not illustrated) must fulfil the periodicity conditions.

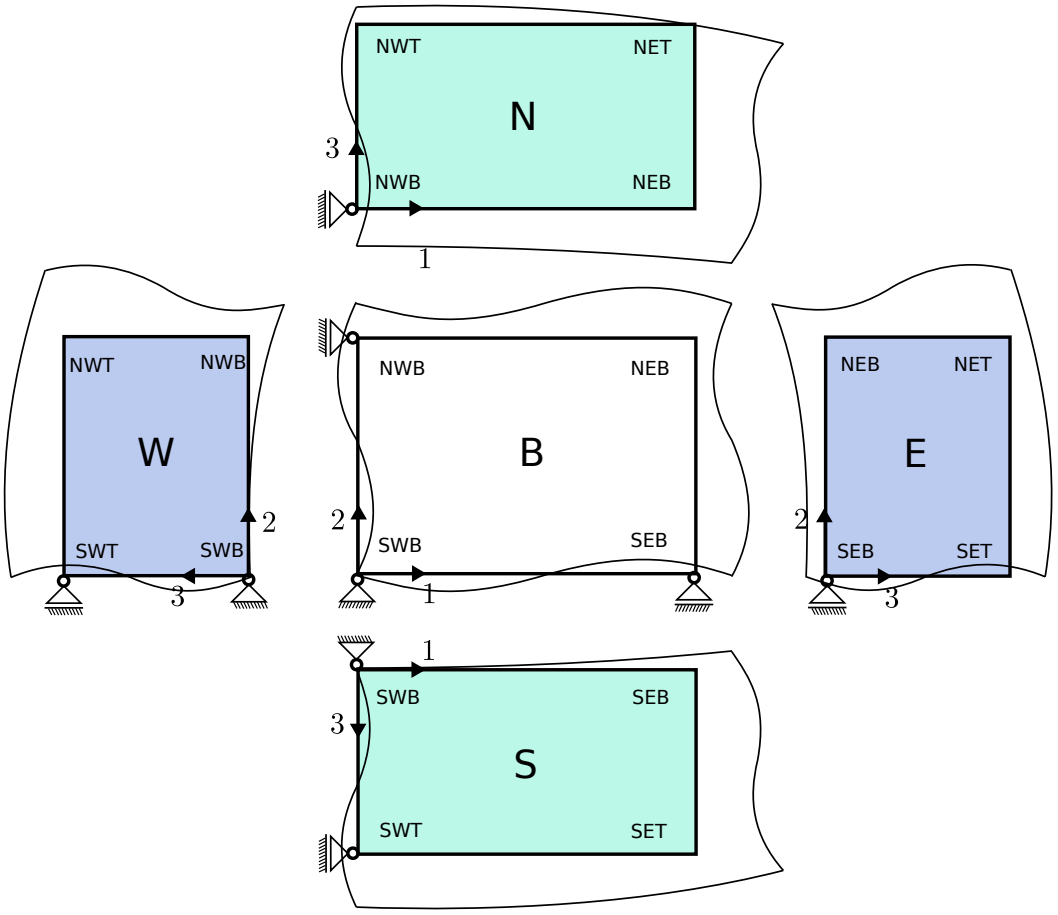


**Figure 3.8:** Schematic illustration of the possible deformation of the unit cell describing the infinite plate

### Semi-infinite plate

In order to model a semi-infinite periodic arrangement and consider free edge effects, periodicity in only one axis is imposed. Within the present framework the face E is chosen to be the free edge and no strain periodicity of the faces W and E is required. For the faces N and S strain compatibility in all three axes is considered. Furthermore symmetry boundary conditions are applied to the face W($u_1^W = 0, \phi_2^W = 0, \phi_3^W = 0$).

Fig. 3.9 shows a possible deformation state of the faces S, N, E, W and B. In contrast to the illustration of the infinite plate deformation, a compatible deformation of the

faces W and E is not required. The 2-3-plane with the distance in direction "1" being zero, represents face W, where the symmetry boundary conditions are applied.

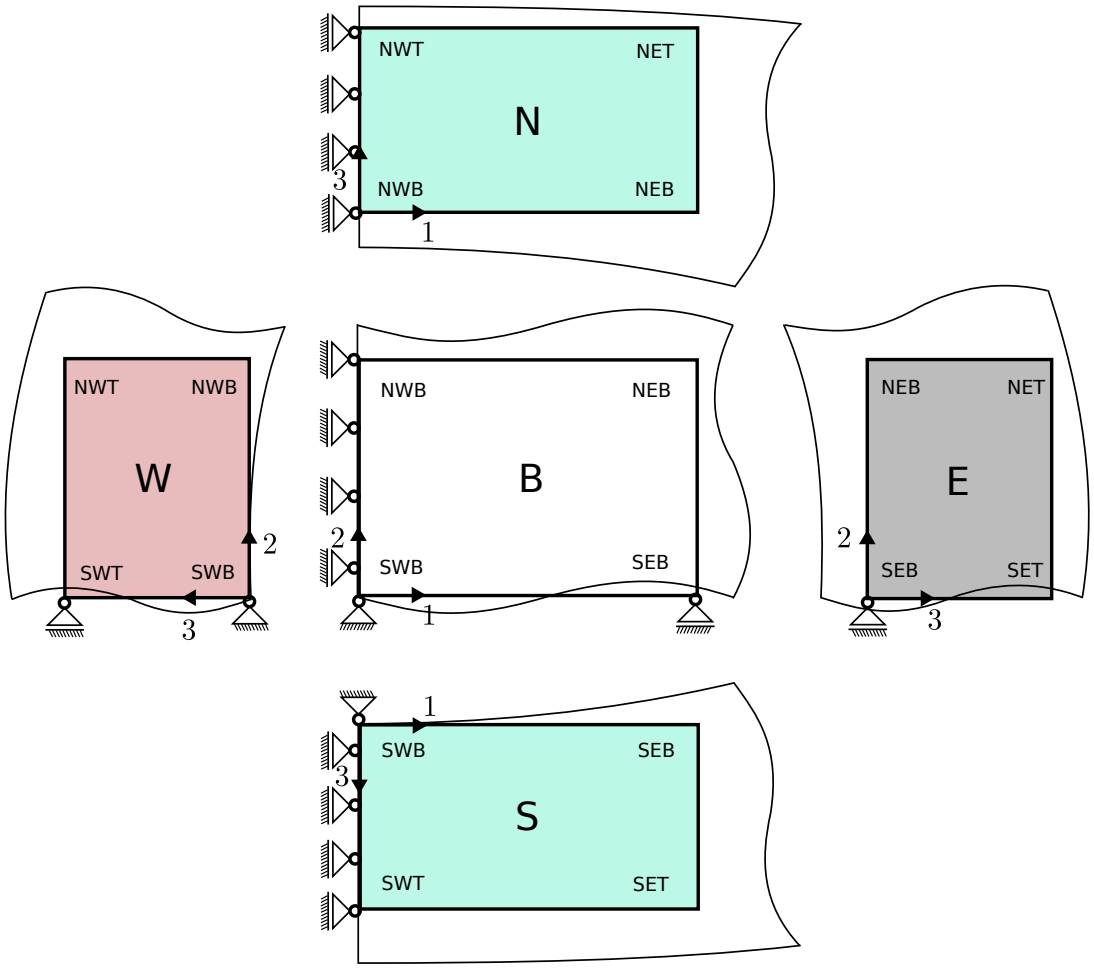


**Figure 3.9:** Schematic illustration of the possible deformation of the unit cell describing the semi-infinite plate

## 3.4 Load Cases

In Section 2.2 the origins of residual stresses induced during the manufacturing process of multilayer coatings are described. To simulate the residual stresses two independent load cases are considered in the following. The stress magnitudes can be varied and combined according to the manufacturing conditions.

### 3.4.1 Thermal Stresses

The residual stresses after the manufacturing process due to the elevated deposition temperature is simulated. To accomplish this, an initial condition of the type temperature is applied to the entire system. Subsequently it is cooled down to room temperature, resulting in thermal stresses due to the mismatch of thermal expansion coefficients of the substrate and the different layer materials.

### 3.4.2 Film Growth Stresses

For simulating the stresses induced by film growth, typical stress magnitudes resulting from the PVD process are applied. In order to implement these stresses in the FE-simulation, an *Abaqus* modelling technique called *model change* is used. It allows to set the stiffness of selected elements to almost zero.
With this method the layers are "removed" in a first step. Then the layer closest to the substrate is prestressed by applying an initial condition of the type stress and is "added" to the system in a second step. This procedure is repeated until the deposition of all layers is completed.

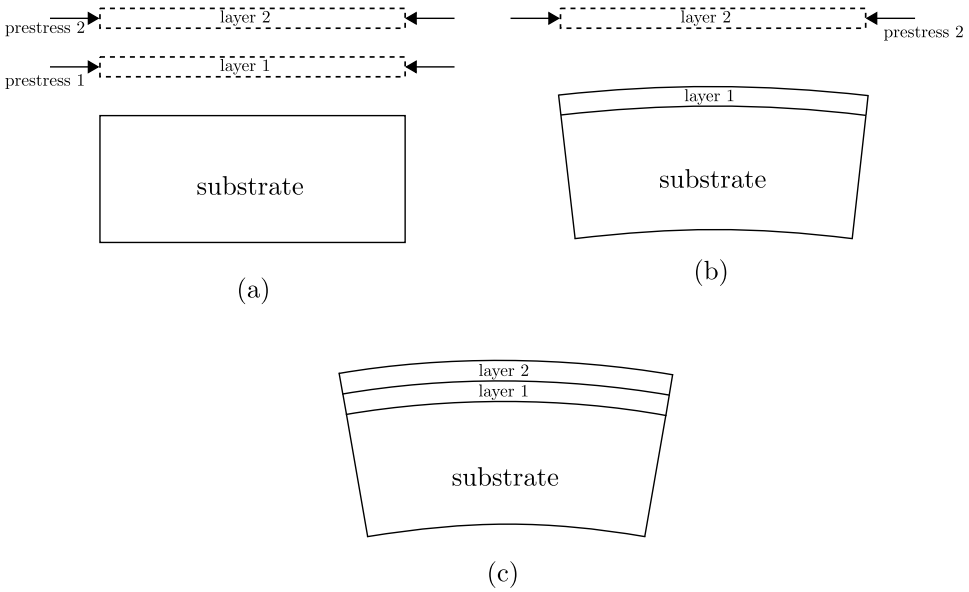


**Figure 3.10:** Schematic illustration of the deposition of two prestressed layers with the modelling technique *model change*

# Chapter 4

# Computational Results

In this chapter the results of the computational simulations are visualised and discussed after a short overview of the considered dimensions and architecture of the multilayer system studied and the pertinent material properties.
A comparison of different discretizations and a verification of the infinite plate model is executed in the ensuing sections.
Using the infinite plate model, the influence of varying materials and process parameters on the stress distribution in multilayer coatings is analysed.
Finally the applicability of the semi-infinite plate model to resolving the stress distribution near a free edge is investigated.
Within this chapter the origins of the stresses are represented by three load cases:

- Load case 1: Thermal stresses
- Load case 2: Film growth stresses
- Load case 3: Total residual stresses

## 4.1 Dimensions and Material Properties

The coatings considered in this study consist of two or three different coating materials deposited alternately on a substrate material. For the substrate a thickness $t_s$ of 380 $\mu$m is considered and the total thickness of the coating $t_c$ ranges from 1 to 10 $\mu$m. For the presentation of the results the coordinate system is chosen to have its origin at the interface between the substrate and the first layer with the $z$-axis being orientated to the coating, Fig. 4.1. Furthermore the definition of a positive and negative curvature chosen for this study is illustrated.

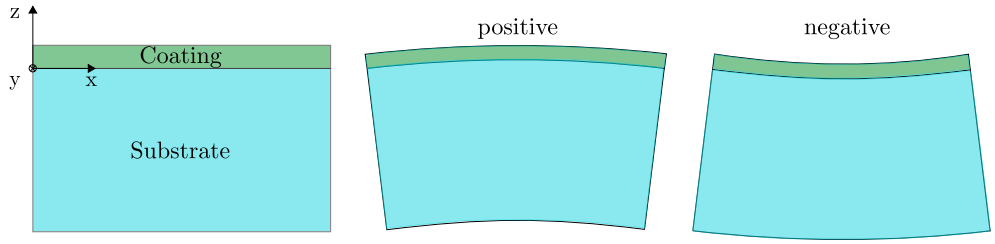


**Figure 4.1:** Position of the coordinate system and definition of positive and negative curvature

For the present study typical substrate and coating materials for multilayer systems are considered. The material properties used within this framework have been provided by the Institute of Materials Science and Technology of TU Wien.

The substrate and the layer materials are assumed to be isotropic and linear elastic. For the substrate this is a reasonable assumption if we only consider polycrystalline materials. The layer materials can be assumed to behave transversally isotropic. The in-plane properties of a polycrystalline material can be described with isotropic properties. Out-of-plane the behaviour can be assumed to be isotropic if we do not consider epitaxial growth of the coating.

When modelling a multilayer system, one has to keep in mind that the microstructure of the film is highly dependent on deposition process parameters, see Section 2.2.1. Hence, the made assumptions might be inappropriate when varying the process parameters.

However, using the presented model also anisotropic material and plasticity can be simulated, but since the results are compared with an analytical approach, only isotropic, linear elastic material behaviour is considered within this study.

### 4.1.1 Elastic Properties

The elastic properties of an isotropic material are defined by two parameters, e.g., the Youngs modulus and the Poisson's ratio. In Table 4.1 the elastic properties for the materials used within this framework are given. The considered substrate materials are an austenitic stainless steel, referred to as Austenite in the following, a Titanium alloy (Ti6Al4V) and Tungsten Carbide-Cobalt (WC-Co). The latter one can only be modelled with isotropic material behaviour if the length scale of the WC-particles can be assumed to be very small.

**Table 4.1:** Elastic properties of the coating and substrate materials

| **Layer material** | **Young's modulus** | **Poissons ratio** |
|---|---|---|
| TiN | 450.0 GPa | 0.216 |
| CrN | 363.0 GPa | 0.257 |
| AlN | 505.0 GPa | 0.166 |
| **Substrate material** | **Young's modulus** | **Poissons ratio** |
| Austenite | 200.0 GPa | 0.3 |
| Ti6Al4V | 110.0 GPa | 0.3 |
| WC-CO | 600.0 GPa | 0.22 |

The multilayer coating might also be represented by a single layer with homogenized properties.

To determine the elastic properties of a homogenized layer diverse models exist in the literature. Based on the assumption that no interfacial sliding occurs between the individual layers when an in-plane stress is applied (Voigt model) the homogenized stiffness can be determined simply by a weighted mean of the Young's moduli of the

components. The homogenized Young's modulus $E_{\mathrm{H}}$ and the Poisson's ratio $\nu_{\mathrm{H}}$ for

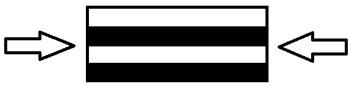

**Figure 4.2:** Voigt model assuming equal strain of the individual layers

a bilayer system is calculated in the following way:

$$E_{\mathrm{H}} = v_{\mathrm{A}}\nu_{\mathrm{A}} + v_{\mathrm{B}}E_{\mathrm{B}} \tag{4.1}$$

$$\nu_{\mathrm{H}} = v_{\mathrm{A}}\nu_{\mathrm{A}} + v_{\mathrm{B}}\nu_{\mathrm{B}} \tag{4.2}$$

where $E_{\mathrm{A}}$ and $E_{\mathrm{B}}$ are the Young's moduli and $\nu_{\mathrm{A}}$ and $\nu_{\mathrm{A}}$ are the Poisson's ratios of the layer material A and layer material B, respectively. The parameters $v_{\mathrm{A}}$ and $v_{\mathrm{B}}$ are the volume fractions of the layer materials.
For the determination of the elastic properties of a homogenized layer an example is given for the case of a TiN/CrN bilayer system with the volume fractions of TiN and CrN being chosen as $v_{\mathrm{A}} = 0.4$ and $v_{\mathrm{B}} = 0.6$, respectively. Applying the rule of mixture leads to the following equation for the Youngs modulus of the homogenized layer.

$$E_{\mathrm{H}} = 0.4 \cdot 450\,\mathrm{GPa} + 0.6 \cdot 363\,\mathrm{GPa} = 397.8\,\mathrm{GPa} \tag{4.3}$$

The calculation of the Poisson's ratio follows the same procedure, leading to

$$\nu_{\mathrm{H}} = 0.4 \cdot 0.216 + 0.6 \cdot 0.257 = 0.2406 \tag{4.4}$$

For the elastic properties of the cohesive zones between the substrate and the first layer the data of the corresponding layer material is used. The elastic behaviour of the cohesive zones between the individual layers is calculated by a rule of mixture. This way the ability of the shell elements to resolve in-plane stresses is extended by the ability of the cohesive elements to capture out-of-plane stresses.

### 4.1.2 Coefficients of Thermal Expansion

The thermal expansion characterization of the layers and the substrate is of great importance, since the mismatch defines the thermal residual stress state of the system. In the analysis the temperature dependence of the coefficients of thermal expansion is considered for the layer materials. For the homogenized layer the CTE is calculated via the following equation:

$$\alpha_{\mathrm{H}} = \frac{\nu_{\mathrm{A}}\alpha_{\mathrm{A}}E_{\mathrm{A}} + \nu_{\mathrm{B}}\alpha_{\mathrm{B}}E_{\mathrm{B}}}{\nu_{\mathrm{A}}E_{\mathrm{A}} + \nu_{\mathrm{B}}E_{\mathrm{B}}} \tag{4.5}$$

This assumption is reasonable due to the strain coupling of the individual layers.
The CTEs were provided by the Institute of Materials Science and Technology as instantaneous values as a function of the temperature in $K$ obtained from ab initio simulations, Fig. 4.3 (a). For *Abaqus* analysis the data has to be changed to total values of the CTE as a function of the temperature in $°C$. This is achieved by integration of the differential values, as stated in Section 2.2.2, which is carried out numerically for the present study. Furthermore the reference temperature was chosen to be $20°C$ which will be taken into account during the analysis. Fig. 4.3 (b) shows the total CTEs of the layer materials used in the analysis.
The thermal expansion of the substrate materials is assumed to be constant with the values given in Tab. 4.2.

**Table 4.2:** CTE values of the substrate materials

| **Substrate material** | **CTE** |
|---|---|
| Austenite | $16.5 \cdot 10^{-6}\mathrm{K}^{-1}$ |
| Ti6Al4V | $9.7 \cdot 10^{-6}\mathrm{K}^{-1}$ |
| WC-CO | $5.5 \cdot 10^{-6}\mathrm{K}^{-1}$ |

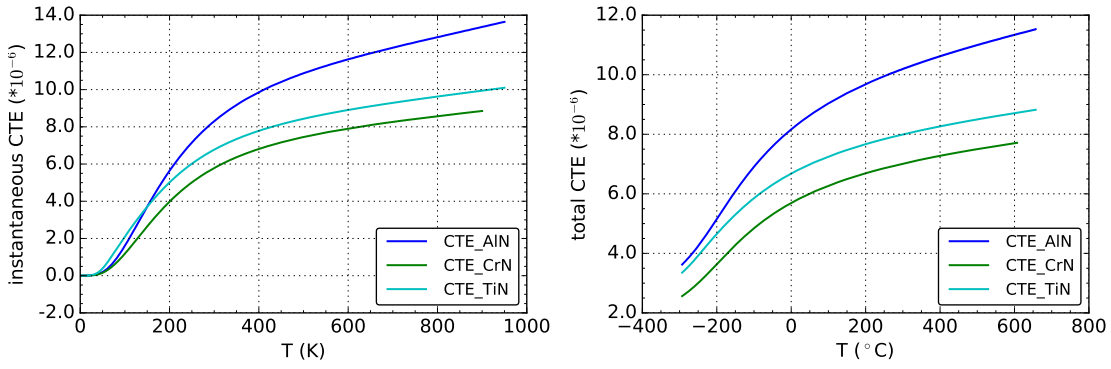


**(a)** **(b)**

**Figure 4.3:** Coefficient of thermal expansion for the different coating materials defind as (a) instantaneous values obtained from ab initio simulations over temperature in $K$ and (b) total values needed for Abaqus analysis over temperature in $°C$ with $T_{ref} = 20°C$

## 4.2 Results of the infinite plate model

Within this Section the results obtained from the infinite plate model are presented. After a short discussion of the required discretization, a verification of the model and a comparison of the layer modelling techniques are carried out. Subsequently a reference configuration of a multilayer system is considered and general remarks concerning the stress distribution are made. Furthermore, the influence of a variation of several parameters on the residual stress distribution is investigated.

### 4.2.1 Discretization of the infinite plate model

This Section should clarify what mesh resolution is needed for sufficiently resolving the stress distribution in the substrate and the layers in the case of the infinite plate model. The dimensions of the multilayer system and the architecture are chosen as shown in Table 4.3, resulting in a total coating thickness of $1\mu$m. A thermal loading of $\Delta T = -480°C$ is applied.

**Table 4.3:** Dimensions and architecture for the mesh size comparison

| | **Material** | **thickness** | **number** |
|---|---|---|---|
| Layer a | TiN | $200nm$ | 2 |
| Layer b | CrN | $300nm$ | 2 |
| Substrate | Austenite | $380\mu$m | 1 |

Three different mesh sizes, referred to as coarse, medium and fine (Table 4.4), are compared. The total number of Elements results from the of continuum elements in the substrate, shell elements representing the layers and the cohesive elements between the substrate and the coating and between the individual layers. For the medium discretization model it can be calculated as follows:
9·9·6 continuum elements + 9·9·4 shell elements + 9·9·4 cohesive elements = 1134

**Table 4.4:** Mesh size comparison

| **Model** | **Elements** | **DOFs** |
|---|---|---|
| coarse | 275 | 1296 |
| medium | 1134 | 4500 |
| fine | 83232 | 267696 |

Fig. 4.4 shows the three models with different discretizations in the deformed state.

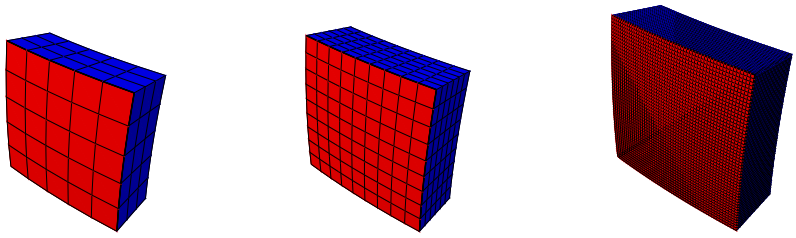

**(a)** **(b)** **(c)**

**Figure 4.4:** Different mesh sizes (a) coarse, (b) medium and (c) fine

Since periodic boundary conditions are applied, the lateral dimensions should be irrelevant and are not changed within this section. In order to keep a reasonable

aspect ratio, a change of the number of elements in-plane results in a change of the mesh size over the substrate thickness. The number of elements in-plane is chosen high enough to sufficiently resolve the curvature.

The stress distribution in the substrate deviates from a straight line at the bottom and the top of the substrate. As can be seen in Fig. 4.5, the deviation is dependent on the discretization since it is the first and the last element where the line has a kink. This is an effect from the *Abaqus* postprocessing. Since reduced integration elements are used for the present simulations, each continuum element has only one integration point. If we choose the output option "*Average element output at nodes*" the results for the node sharing elements are averaged. Due to the fact that at the bottom and the top only one element each accounts for the stress value, which is the result of one integration point, the stress magnitude is underestimated. In the present Chapter a discussion of the qualitative statements of the results is aimed and hence, the deviation due to this error will be tolerated.

Within this Section, the normal stress component of the substrate and the coating in the $xy$-plane will be referred to as substrate in-plane stress $\sigma_S$ and coating in-plane stress $\sigma_C$, respectively.

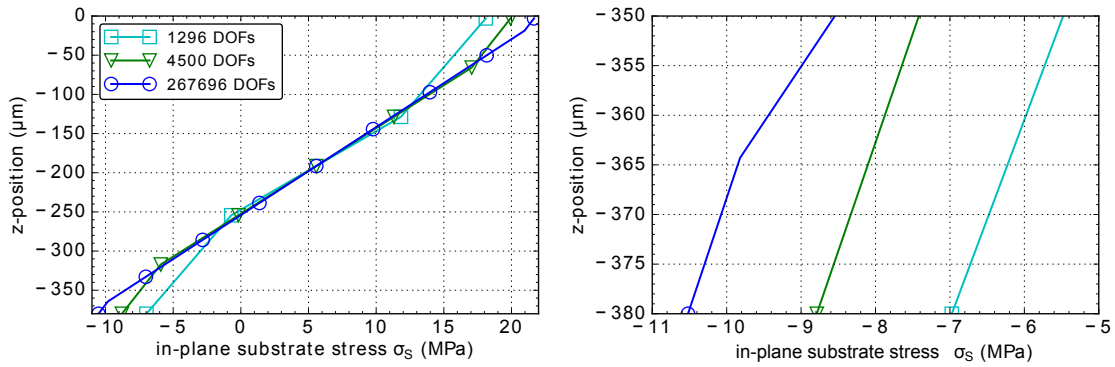


**Figure 4.5:** Stress distribution in the substrate for different discretizations (right: detail)

As can be seen in Fig. 4.6, the results for the coating in-plane stress obtained from the three different mesh sizes correlate very well and the discrepancy over the total

coating thickness keeps constant. The maximum compressive coating stress and the

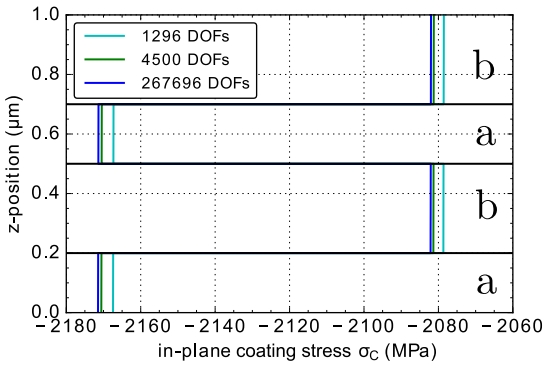


**Figure 4.6:** Stress distribution in the coating for different discretizations

average substrate stress are given as a function of the degrees of freedom (DOF) of the total system, see Fig. 4.7. An excessively small number of elements can not capture the stress distribution over the thickness sufficiently well and underestimate the stress magnitude in the substrate as well as in the coating.

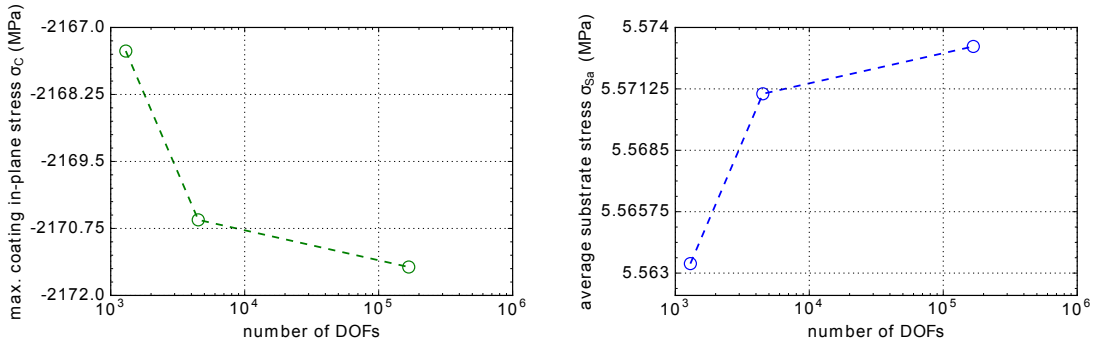


**Figure 4.7:** Influence of number of DOFs for a system with two bilayers on the results for (a) the maximum coating in-plane stress (b) the average substrate stress

Since the percentage difference between the medium and fine discretization amounts to less than 0.1% for the maximum compressive coating stress and the average in-plane substrate stress, the medium discretization is considered to be an adequate compromise regarding a good resolution and little computational time. Therefore it

is chosen as the reference configuration within this thesis.

### 4.2.2 Verification of the infinite plate model

In order to verify the three dimensional FE-Model of the infinite plate, it is compared with an analytical approach, based on the Bernoulli beam theory applied to an inhomogenous beam [20]. In order to ensure comparability between the analytical approach and the infinite plate model, the material behaviour has to be considered as isotropic and linear elastic. Furthermore, a biaxial Young's modulus was taken into account in the analytical approach.
For the comparison with the analytical approach the dimensions used in Subsection 4.2.1 are considered, but instead of 2 bilayers, 20 bilayers are deposited, resulting in a total coating thickness of 10$\mu$m. For a better readability of the diagrams, only the stress distribution in the individual layers obtained by the analytical model is plotted. The FE-model results, in contrast, are plotted over the entire coating thickness including the stress changes between the layers within this Section.

#### Load case 1

For the simulation of the stresses due to the mismatch of coefficients of thermal expansion, a thermal loading of $\Delta T = -480°C$ is applied. In Fig. 4.8 (a) the stress distribution over the total thickness is plotted, whereas Fig. 4.8 (b) shows the details of the stress distribution in the first four layers.

The results for the in-plane stress in the individual layers obtained by the analytical model and the FE-model correspond fairly well. The relative difference amounts around 0.4% and keeps constant over the thickness.

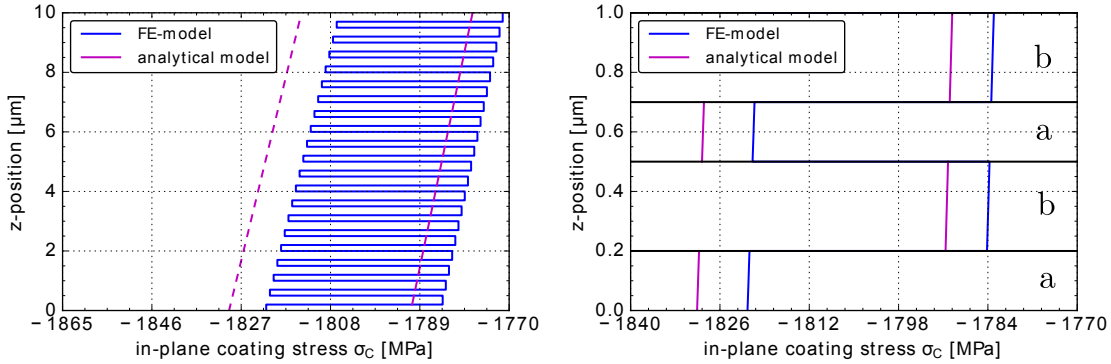


**Figure 4.8:** Analytical and numerical results for the in-plane stress of the individual layers due to thermal loading (right: detail)

### Load case 2

To simulate the film growth stresses, a prestress of $\sigma_p = 3\text{GPa}$ is applied to each individual layer. Fig. 4.9 shows a similar relative difference in terms of the predicted residual stresses as was found for the load case 1.

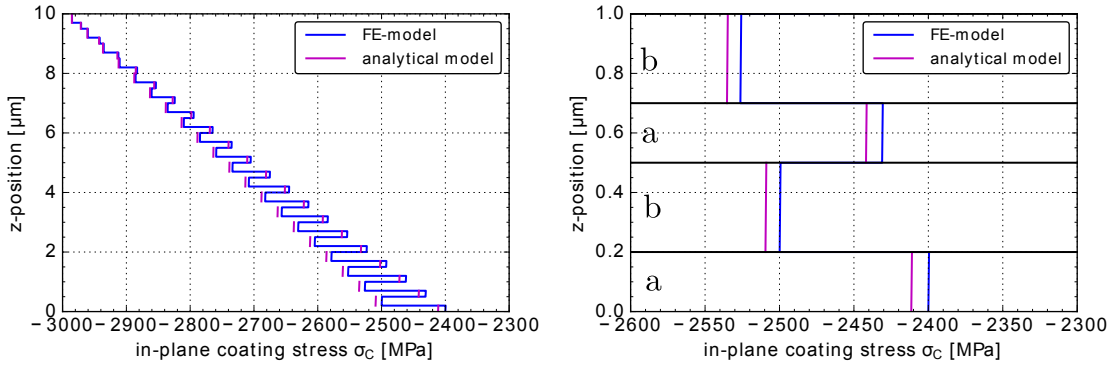


**Figure 4.9:** Analytical and numerical results for the in-plane stress of the individual layers due to film growth (right: detail)

### Load case 3

For the simulation of the total residual stress state in the coating, both, a prestress of $\sigma_p = 3\text{GPa}$ to each layer and a thermal loading of $\Delta T = -480°C$ to the entire system is applied. Due to the fact that for both load cases the numerical simulation

predicts lower in-plane stresses of approximately 0.4% and the simulations are carried out without considering non-linearities, also the superposition of the two load cases lead to a percentage difference of 0.4%.

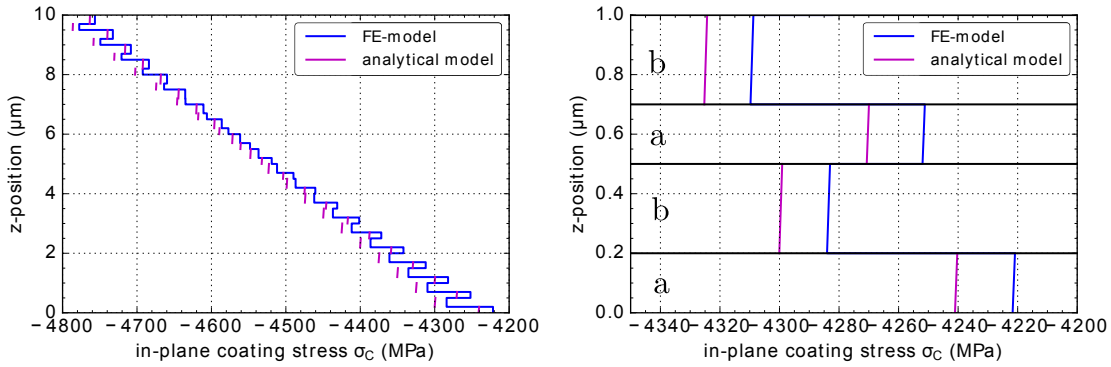


**Figure 4.10:** Analytical and numerical results for the in-plane stress of the individual layers due to film growth and thermal loading (right: detail)

Concluding it can be stated, that both approaches give comparable results. Hence, the developed infinite plate model can be considered as an adequate tool for predicting the stress distribution in a multilayer system with the assumptions made.

### 4.2.3 Comparison of modelling techniques

In this Section the three layer modelling techniques described in Section 3.2 are checked for their applicability to investigating the residual stress distribution in a multilayer system. To do so, the load cases 1 and 2 are applied to the infinite plate model. The same dimensions as in Section 4.2.2 are considered.

#### Load case 1

The model is subjected to a thermal loading of $\Delta T = -480°C$. Fig. 4.11 shows the in-plane stress in the substrate and the coating as a function of the $z$-position. As can be seen, the simulations of the individual layers and the composite shell show a good correlation of the results. The coating stress values obtained from by the model with

one homogenized coating must lie between the the results obtained for individual layers. Since the thickness of layer $a$ and layer $b$ differ, the dotted line, representing the stress in the homogenized layer, does not lie in the middle as the effective elastic properties were determined using a rule of mixture taking into account the volume fraction of the bilayer materials.

The in-plane stress integrated over the total thickness of the coating leads to the same results for the different modelling techniques. Consequently the stress distributions in the substrate obtained by the three techniques are expected to correspond to a high degree. This is consistent with the results for the stress distributions in the substrate shown in Fig. 4.11.

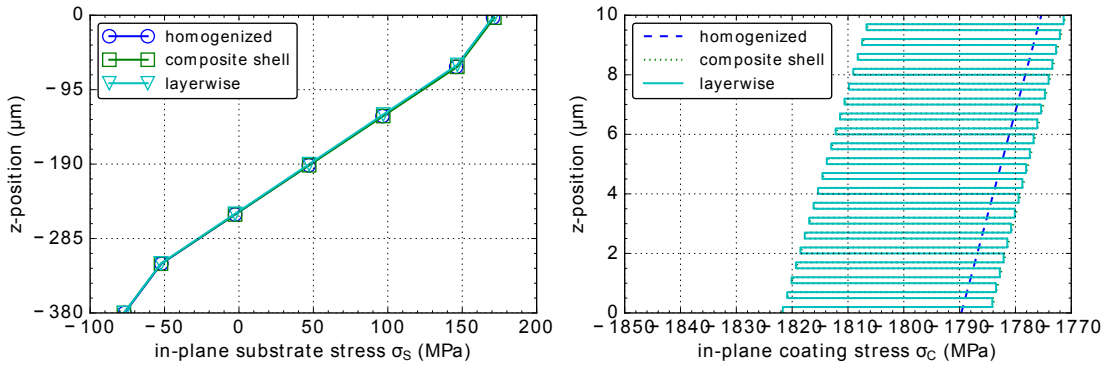


**Figure 4.11:** Comparison of the in-plane stress in the substrate and the coating due to thermal loading obtained by the three different modelling techniques

### Load case 2

In order to simulate the film growth stresses, an initial compressive prestress of 3GPa is applied to the coating. Representing the coating as one thick layer using homogenized properties or modelled with a composite shell, the prestress is applied to the entire coating. After that, the coating is deposited in one single step. In comparison, the layerwise modelling technique deposits the layers successively after applying the prestress to each single layer.

As depicted in Fig. 4.12, the results for the residual stress state in the substrate and

the coating obtained by the homogenized layer and composite shell lie in the same range. This is due to the fact, that for both modelling techniques, the prestress is applied to the coating at once. Only the material properties vary layerwise within the composite coating.

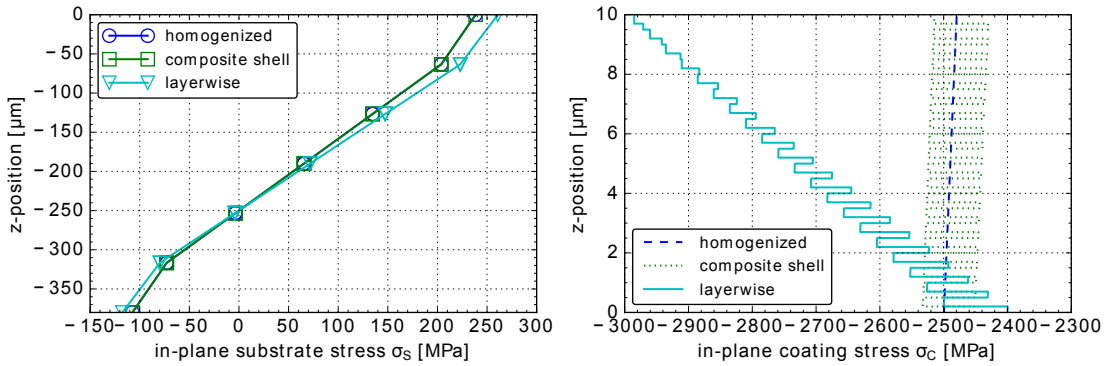


**Figure 4.12:** Comparison of the in-plane stress in the substrate and the coating due to film growth obtained by the three different modelling techniques

Due to the fact, that only linear elastic material behaviour is considered, one might assume, that the results of the layerwise deposition coincides with the composite shell stress distribution. This is not the case for the simulation of the present problem, as can be seen from the results of the stress distribution in the coating obtained from the three different modelling techniques. A high discrepancy between the layerwise deposition and the other two modelling techniques can be observed. When depositing the coating in one step, bending induces tensile stresses which decrease the magnitude of the applied prestress. If the layers are deposited one by one the overall stiffness of the system and the neutral axis changes after each deposition step. Subsequently, the system adjusts towards a new equilibrium. Due to bending of the substrate and the coating, this leads to additional tensile stresses in the previously deposited layers. However, since the layers are deposited with the total prestress on the already deformed system, the tensile stress in the present layer is induced only by the change in curvature due to its deposition and not by the total system curvature. Consequently, also the result for the stress distribution in the substrate deviates from

the other modelling techniques.
On the basis of this information, it can be said, that a homogenization of the individual layers with one single layer is not appropriate for the present study.

### 4.2.4 Reference configuration and general remarks

In order to point out general observations made on the results for the residual stress distribution in multilayer coatings obtained from the infinite plate model, a reference configuration with the dimensions and architecture listed in Tab.4.5 is considered. To simulate the thermal mismatch stress a thermal loading of $\Delta T = -480°C$ is applied. The film growth process is simulated with a prestress of 3 GPa on each individual layer.

**Table 4.5:** Dimensions and architecture for the reference configuration

| | **Material** | **thickness** | **number** |
|---|---|---|---|
| Layer a | TiN | $200nm$ | 20 |
| Layer b | CrN | $300nm$ | 20 |
| Substrate | Austenite | $380\mu$m | 1 |

In order to improve the readability of the diagrams only the average in-plane stress magnitudes of the individual layers are considered and a linear interpolation between the obtained values over the total coating thickness is plotted. Only for detailed illustrations of the first layers the actual stress distribution is considered.
If isotropic behaviour and uniform loading in the absence of any defects or geometrical variations in the material are considered, the in-plane stresses in both lateral axes have the same magnitude. Consequently the magnitude of the residual stress in an infinite plate is simply a function of the z-position. As mentioned in Chapter 3, stretching and in-plane shearing of the midsurface of a cohesive element does not generate any interfacial stresses. Hence, in the case of an infinite plate without a free edge no stresses are induced in the interface.
In Fig. 4.13 the stress distribution in the substrate and the coating due to the three

different load cases is plotted. A comparison of the residual stress state in the substrate and the coating indicates a much higher stress level in the coating. This is primarily due to the small ratio of the coating to substrate thickness and the necessity to fulfil the force and moment equilibria.

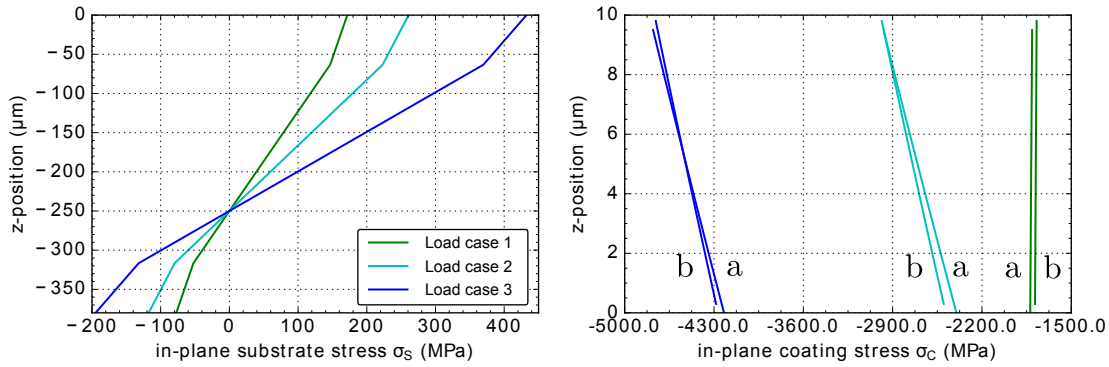


**Figure 4.13:** Residual in-plane stress of the substrate and the coating due to the different load cases

For the chosen reference configuration, the thermal mismatch stress leads to a compressive residual stress in the coating. As a consequence, the stress state in the substrate is positive at the top and negative at the bottom. Applying a prestress representing the film growth stresses further puts the coating in a compressive state, leading to the same effect as the thermal loading in the substrate. Both load cases result in a positive curvature of the system. Since no non-linearities are considered in this simulation, the results obtained for the load case 3 can be considered as the superposition of the film growth stresses and the thermal stresses. Thus, also the final curvature of the system is positive. For the chosen configuration the contributions of the two load cases to the total residual stress state, however, are in the same range. This can be very different for different material properties and loadings as will be discussed in the next section.

In Fig. 4.14 a detailed presentation of the stress distribution in the first four layers resulting from load case 1 is plotted. The in-plane coating stress distribution indicates, that the stress magnitude decreases with a higher $z$-position. That is because the positive curvature of the system induces a higher magnitude of tensile stress in the

layers with a greater radius of curvature. Furthermore the diagram suggests that the layer material with the higher Young's modulus (TiN) exhibits a higher compressive stress. Generally it can be said, that a material with a CTE closer to that of the substrate material experiences smaller in-plane strains and hence, smaller stresses. This applies to TiN in the considered reference configuration. However, a higher compressive stress is observed for this layer material and hence, it can be deduced that the influence of a higher Young's modulus has a dominating effect in the present configuration.

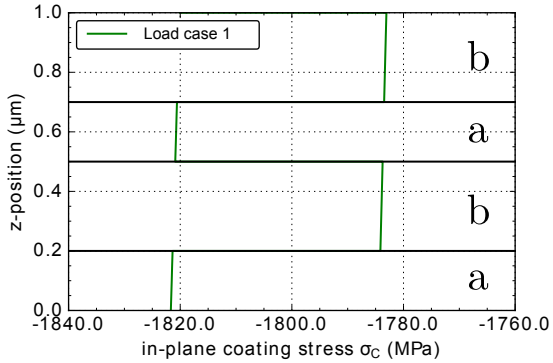


**Figure 4.14:** Residual in-plane stress of the first four layers due to thermal loading

The stress distribution in the first four layers obtained when applying load case 2, representing the film growth stress, is depicted in Fig. 4.15(a). It indicates that the compressive stress level increases with a higher $z$-position. This results from the effect of layerwise deposition discussed in Section 4.2.3. In contrast to load case 1, a higher Young's modulus of the layer material leads to a lower stress level when applying a prestress. This is because the magnitude of the applied prestress is chosen independent of the material properties, whereas the stresses due to the induced bending of the sample are highly dependent on the elastic properties of the material.

For the chosen reference configuration the total residual stress state in the first four layers is depicted in Fig. 4.15(b).

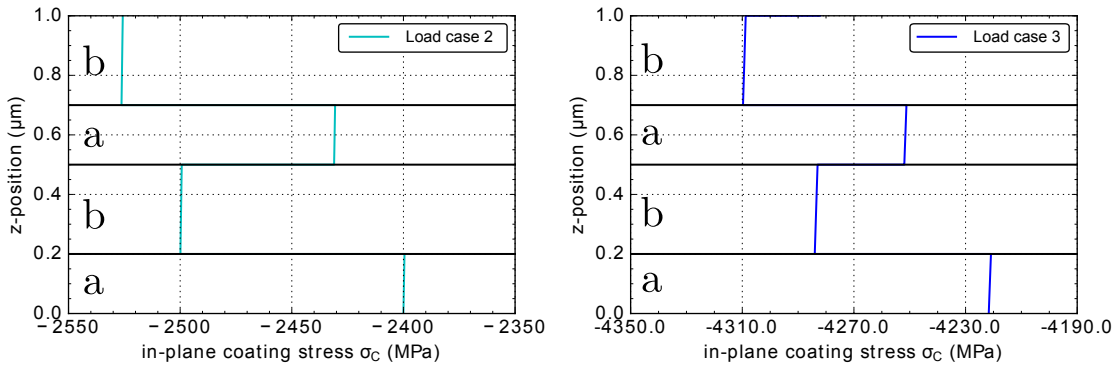


**(a)** **(b)**

**Figure 4.15:** Residual in-plane stress of the first four layers due to (a) film growth and (b) film growth and thermal loading

### 4.2.5 Influence of parameters

In this section the influence of several parameters on the stress distribution in the multilayer system is discussed. In order to do so, the reference configuration with the indicated dimensions and loadings is considered and the parameters are varied separately.

#### Variation of the substrate material

The influence of changing the substrate material on the residual stress state in the coating and substrate is investigated here. The considered materials are Austenite, Tungsten Carbide-Cobalt (WC-Co) and a Titanium alloy (Ti6Al4V). When the substrate material is varied, both, the change of CTE and the change of the elastic properties, influence the resulting stress distribution independently.

In Fig. 4.16 the stress distribution in the substrate and the coating is plotted for the case of thermal loading. Considering the substrate material with a lower CTE than the coating materials, in this case WC-Co, results in a negative curvature of the sample. If the CTE of the substrate material is in approximately the same range as the CTE of the layer materials, a low stress level is achieved. This is the case when

Ti6Al4V is considered. A decrease of the magnitude of residual stress in the substrate lowers the stress level in the coating too. The influence of the three different substrate

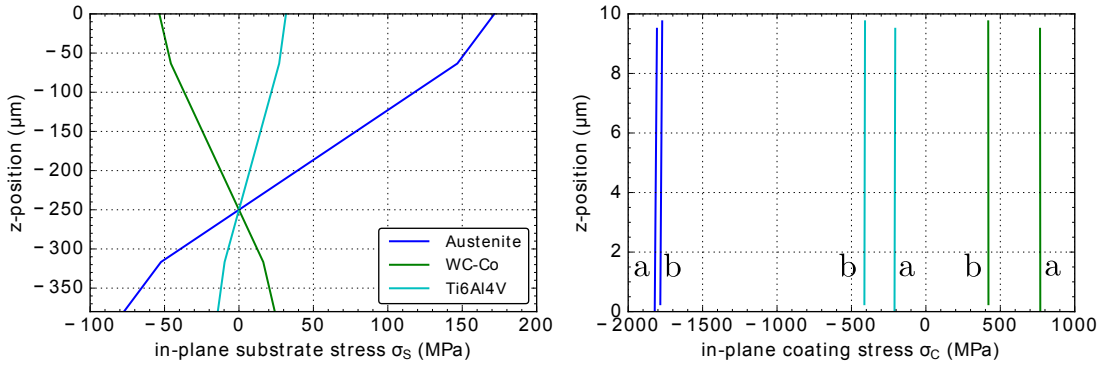


**Figure 4.16:** Influence of the variation of the substrate material on the in-plane stress of the substrate and the individual layers due to thermal loading

materials on the residual stress state due to film growth stresses in the substrate and the coating is depicted in Fig. 4.17. Considering WC-Co, being the material with the highest Young's modulus considered in this study, increases the substrates resistance against in-plane deformation and its bending stiffness. Consequently, less of the initially applied prestress in the coating can be relieved by elongation and bending of the system.

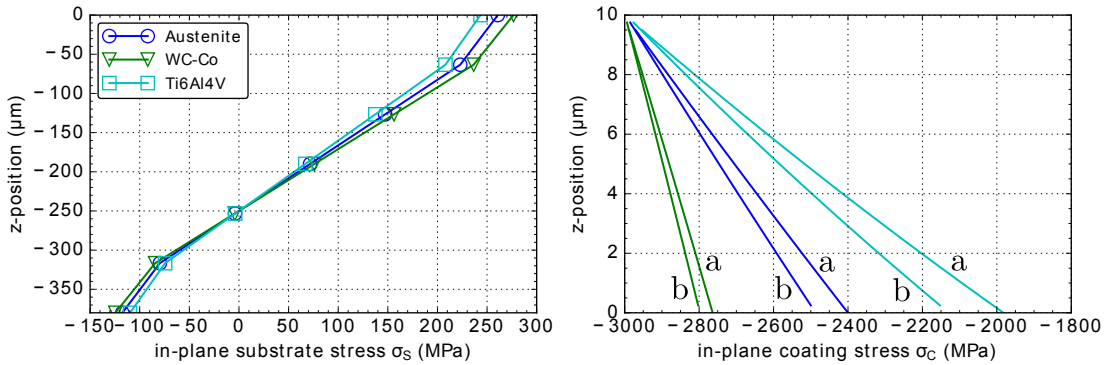


**Figure 4.17:** Influence of the variation of the substrate material on the in-plane stress of the substrate and the individual layers due to film growth

Fig. 4.18 shows the total residual stress distribution in the substrate and the coating for the different substrate materials. The stress distribution due to film growth stress lies in the same range for all three materials, whereas the thermal mismatch stress can be varied drastically by changing the substrate material. If a substrate with a lower CTE than the coating material is used, the compressive residual stress can be reduced to a high degree. Whereas a CTE of the substrate higher than those of the coating leads to an accumulation of the film growth and thermal mismatch stress magnitudes.

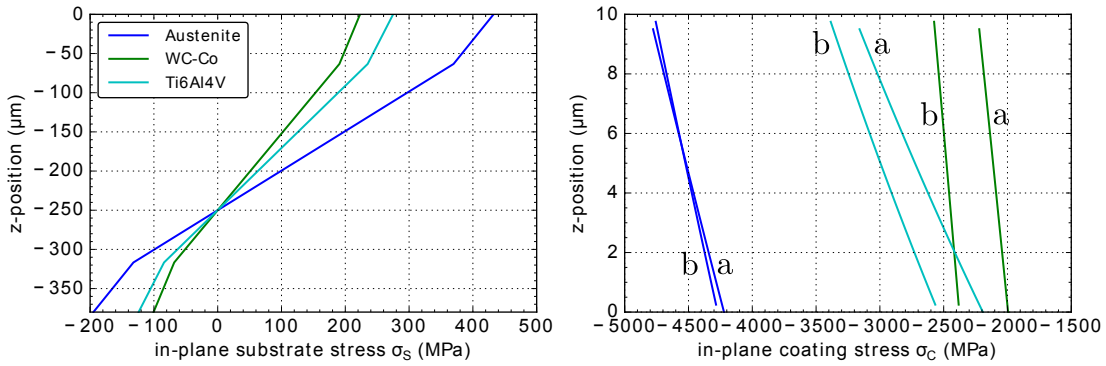


**Figure 4.18:** Influence of the variation of the substrate material on the in-plane stress of the substrate and the individual layers due to film growth and thermal loading

### Variation of the number of individual layers

As discussed in Section 4.2.3, depositing one thick coating results in a very different stress distribution compared to a layerwise deposition of 20 bilayers. In the following it is investigated, whether the number of individual layers still has a great influence if we consider 20, 100 and 500 bilayers, each having the same total coating thickness and the same volume fraction of the two coating materials chosen in the reference configuration.

Fig. 4.19 depicts the stress distribution in the substrate and the coating for the three

different cases. In none of the two diagrams, representing the stress distribution in the substrate and the coating, a significant difference between the 20, 100 and 500 bilayer coatings can be observed. Therefore it can be concluded that the deposition of 20 bilayers already results in a very similar stress distribution as the deposition of an infinite number of bilayers. The minimum number of layers which sufficiently approximates the stress level of a certain number of layers might be highly dependent on the material properties and load cases and no general statement can be made.

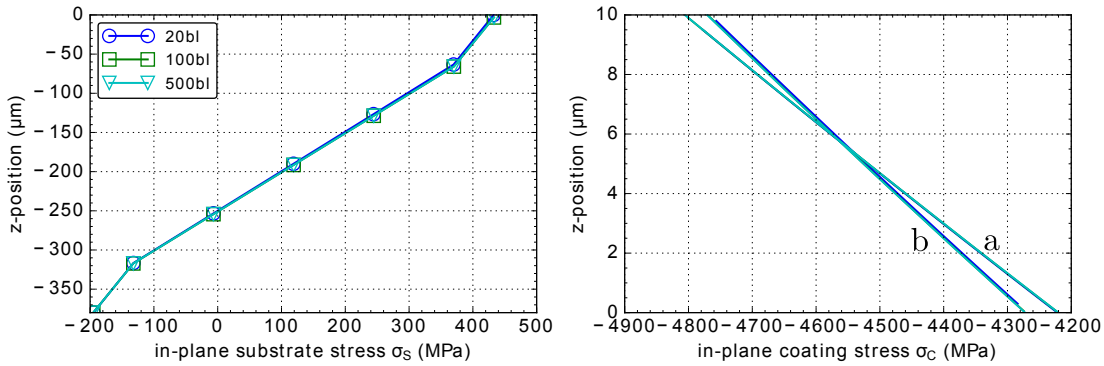


**Figure 4.19:** Influence of the variation of the number of individual layers on the in-plane stress of the substrate and the individual layers due to film growth and thermal loading

### Variation of the coating thickness

In order to investigate the influence of the total coating thickness on the residual stress state, two configurations with the same coating architecture but a differing number of bilayers are considered. The coating consists of 8nm TiN and 12nm CrN layers. A coating of 50 bilayers, $t_C = 1\mu$m, is compared with a coating comprising 500 bilayers, $t_C = 10\mu$m. Fig. 4.20 indicates that a thicker coating decreases the stress magnitude in the layers. The 500 bilayers coating which is 10 times as thick as the 50 bilayers coating results in a reduction of the average residual coating stress of about 12%. In order to fulfil the force and moment equilibria a thicker coating leads to a higher residual stress level in the substrate.

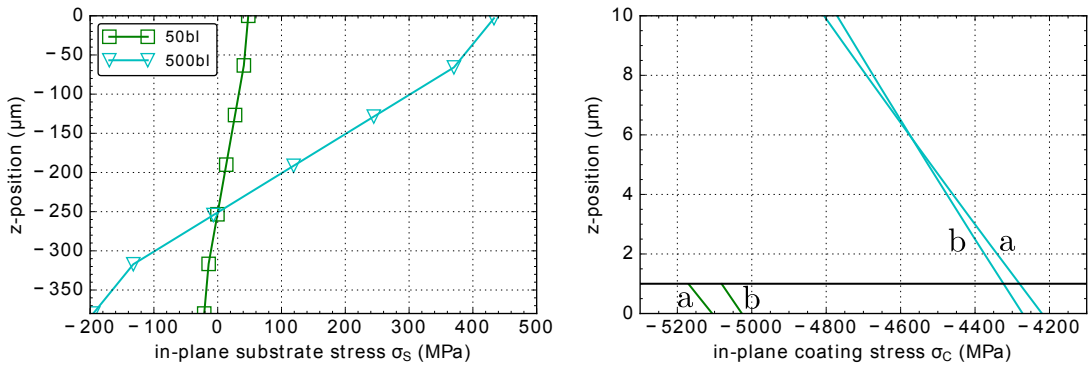


**Figure 4.20:** Influence of the variation of the total coating thickness on the in-plane stress of the substrate and the individual layers due to film growth and thermal loading

### Variation of the layer material

In the following the influence of a different combination of bilayer components is discussed. Two combinations are considered: TiN/CrN and AlN/CrN. The resulting stress distributions in the substrate due to the three different load cases is illustrated in Fig. 4.21. The coating with the higher average CTE, being AlN/CrN in the present comparison, leads to a smaller mismatch of thermal strain between the substrate and the coating. Hence, a lower level of residual stress is generated in the substrate, as can be observed in Fig. 4.21(a). The residual stress distribution due to the prestressed deposition of the layers, representing film growth, shows only a small reduction of the stress magnitudes for the AlN/CrN coating, Fig. 4.21(b). The total residual stress state, Fig. 4.21 (c), shows, that considering AlN/CrN instead of TiN/CrN as the layer materials of the multilayer coating, leads to a lower stress level in the substrate for the chosen configuration.

The residual stress distribution over the total coating thickness is illustrated in Fig. 4.22. The CTEs of TiN and CrN are in the same range and hence, the results for the stress distributions in the two layer materials lie very closely together, see Fig. 4.22 (a). On the other hand, the CTE of AlN is much higher than that of CrN. Consequently, a high discrepancy can be observed for the stress distribution in

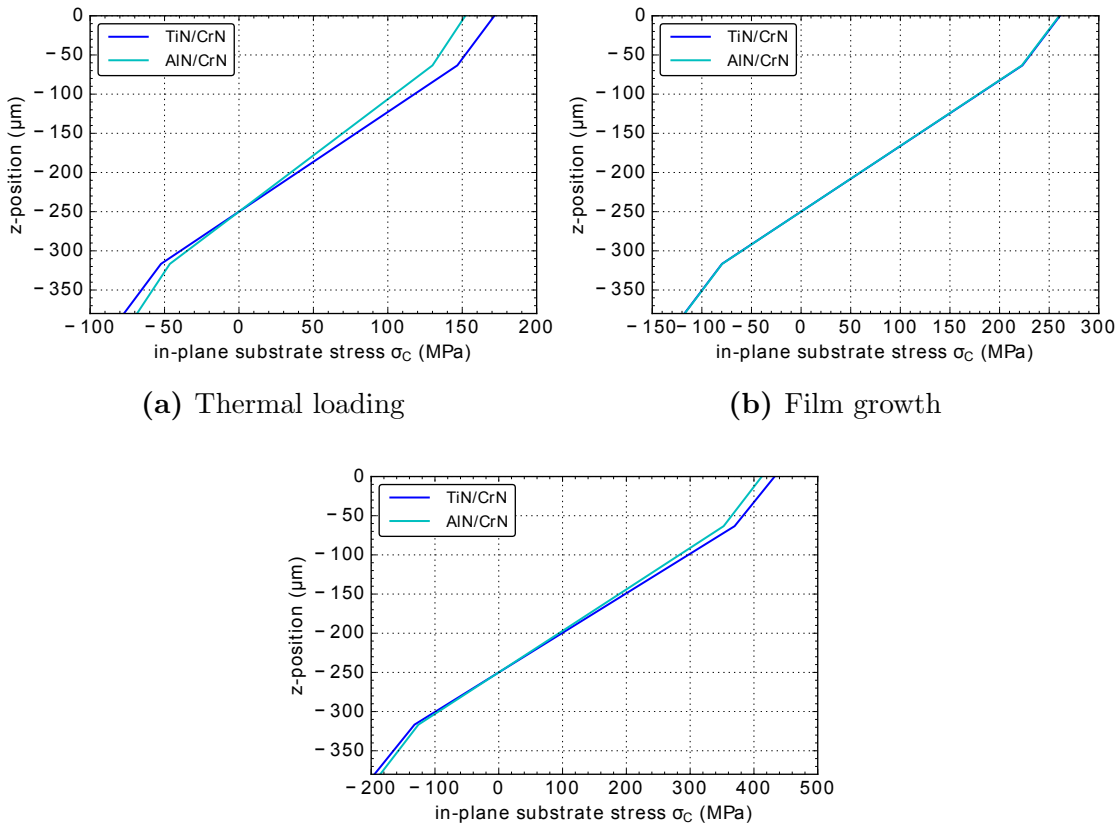


**(a)** Thermal loading

**(b)** Film growth

**(c)** Film growth and thermal loading

**Figure 4.21:** Influence of the variation of the material of one coating component on the in-plane stress of the substrate for the load cases 1-3

the two layers. Since always both layer materials influence the stress distribution in the individual layers, the CrN does not show the same thermal residual stress for the two coating material combinations.

Since AlN has a higher Young's modulus than TiN, a lower stress level due to the prestressed deposition, i.e. film growth stress, is observed in Fig. 4.22 (b). This can be explained by the fact, that the prestress is independent of the elastic properties, whereas the contribution of the tensile stresses due to bending is higher for a higher Young's modulus. For the superposition of the two load cases, Fig. 4.22 (c), it can be said, that for the chosen configuration, using AlN instead of TiN leads to a lower stress level in the layer $a$. However, a greater discrepancy between the stress

magnitudes in the two layer materials is generated, which might be critical for the corresponding interfaces.

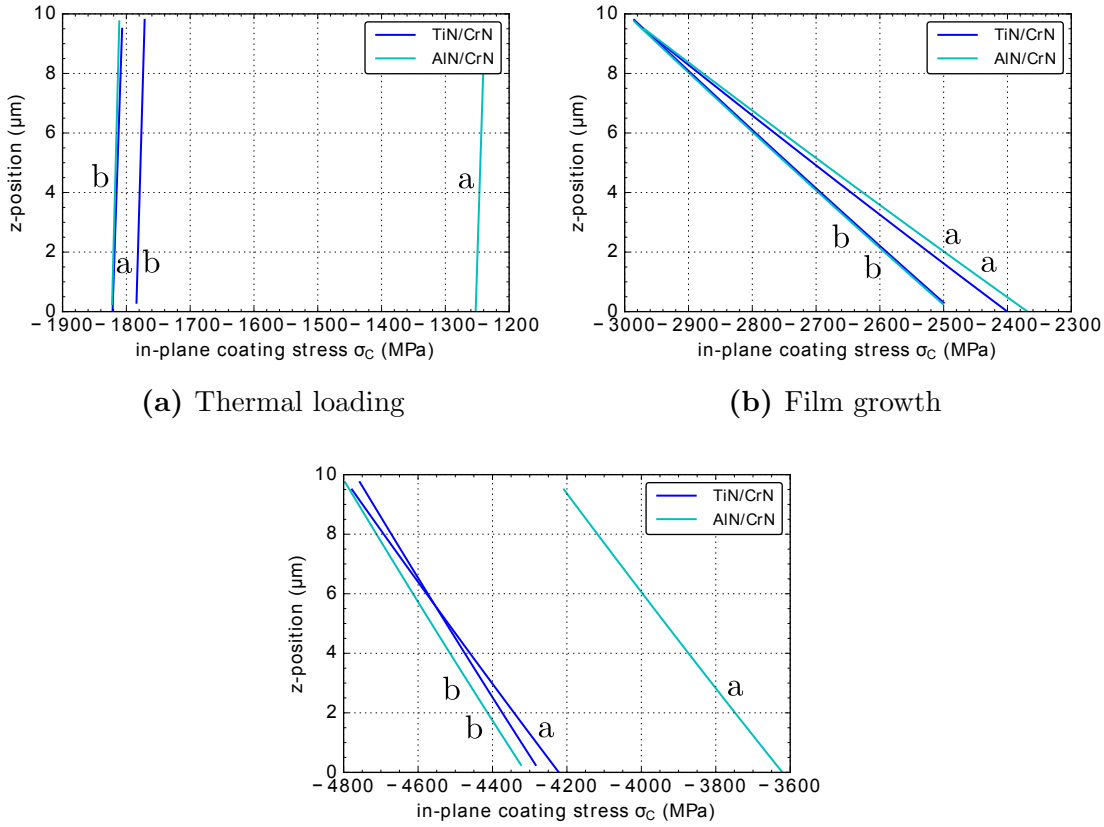


**(a)** Thermal loading

**(b)** Film growth

**(c)** Film growth and thermal loading

**Figure 4.22:** Influence of the variation of the material of one coating component on the in-plane stress of the coating for the load cases 1-3

## 4.3 Results of the semi-infinite plate model

In the following Section the results obtained for the stress distribution of a multilayer system with a free edge are discussed. After a verifying comparison with the infinite plate model, general remarks are made on the resulting stress distribution and the required discretization.

### 4.3.1 Verification of the semi-infinite plate model

The model must be sufficiently long and the mesh sufficiently fine to allow the stresses to decay. Hence, the stress distribution at the face with the symmetry boundary conditions should coincide with the stress distribution in the infinite plate model. Furthermore, due to the assumption of isotropic material behaviour, the stress magnitudes in both in-plane directions must be the same.

At the position where edge effects have already decayed the stress distribution in the layers and the substrate of the semi-infinite model is evaluated and compared with the results obtained by the infinite plate model. The thicknesses and coating architecture from Section 4.2.4 are considered. The lateral dimensions of the semi-infinite plate model are chosen to be 5$\mu$m in the axis of periodicity and 350$\mu$m in the axis with symmetry boundary conditions. The elements dimensions normal to the free surface are chosen to be 0.3$\mu$m.

Fig. 4.23 shows the in-plane stress distribution in the coating due to thermal loading and film growth. There is only a small difference between the results obtained by the two models. Hence, the semi-infinite plate model can also be considered for the evaluation of the stress distribution where the stresses due to edge effects have decayed.

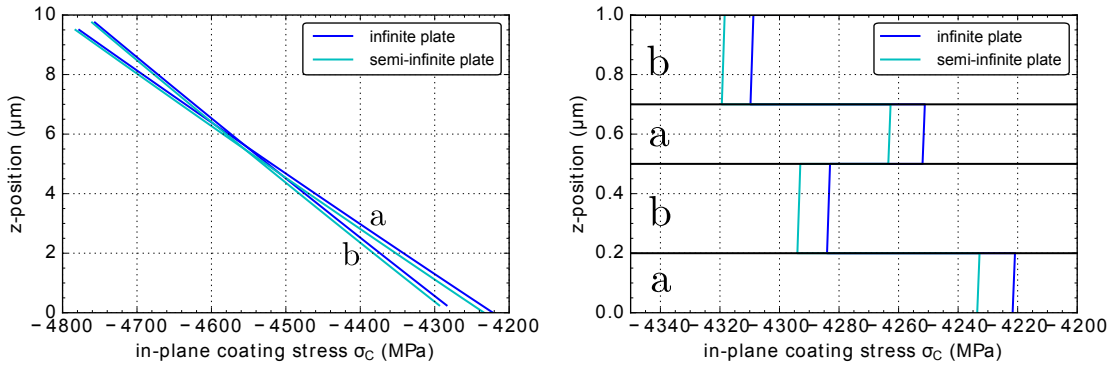


**Figure 4.23:** Results for the in-plane stress of the individual layers due to film growth and thermal loading obtained by the infinite plate model and semi-infinite plate model at the end with symmetry boundary conditions

### 4.3.2 General remarks on the semi-infinite plate results

The in-plane stresses discussed in the previous Sections are transferred to the coating via normal stresses and shear stresses on the interface close to the free edge. This effect can result in mode I and II edge delamination. Furthermore, stresses different to those remote from the edges are induced in the substrate and the coating. These effects are evaluated qualitatively in the following.

#### Influence of a free edge on the stress distribution in the substrate and the coating

The presence of a free edge leads to a different stress distribution in the substrate and the coating close to the free surface compared to the stress distribution remote from the free surface. A set of contour plots pertaining to this discussion can be found in Appendix 1.

Considering the substrate-coating system from Section 4.3.1, a much higher tensile stress level in the substrate is reached in the vicinity of an edge normal to the free surface. Also compressive stresses of a slightly higher magnitude than the ones in the infinite plate model are induced. The in-plane stresses parallel to the free surface have their extreme values close to the free edge, too. Furthermore, out-of-plane normal and shear stresses are induced in the substrate, which are absent in the models without a free edge. The coating, in comparison, shows its maximum compressive stresses remote from the edge in both in plane directions. However, tensile stresses are induced, but with a magnitude lower compared to the compressive stresses.

It can be said, that for the chosen configuration, the compressive stresses in the layers are relieved, whereas the substrate has to withstand much higher stresses in the presence of a free edge.

### Influence of a free edge on the stress distribution in the interface

In Fig. 4.24 and 4.25 the interfacial normal and shear stress distributions, respectively, for the three load cases applied on a system consisting of a 380$\mu$m thick substrate and a single layer with a thickness of 10$\mu$m is depicted. In the right diagrams, a close-up of the region close to the free edge is illustrated. Similar shapes of the interfacial stresses can be observed for load case 1 (thermal mismatch stresses) and load case 2 (film growth stresses). The resulting stress distribution obtained for load case 3 (total residual stresses) is the superposition of the two above load cases.

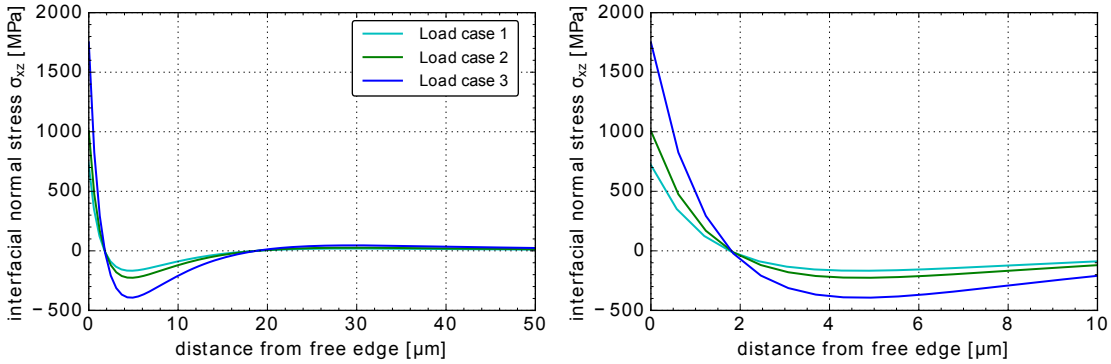


**Figure 4.24:** Interfacial normal stresses for a 1-layer-system subjected to the three load cases (right: detail)

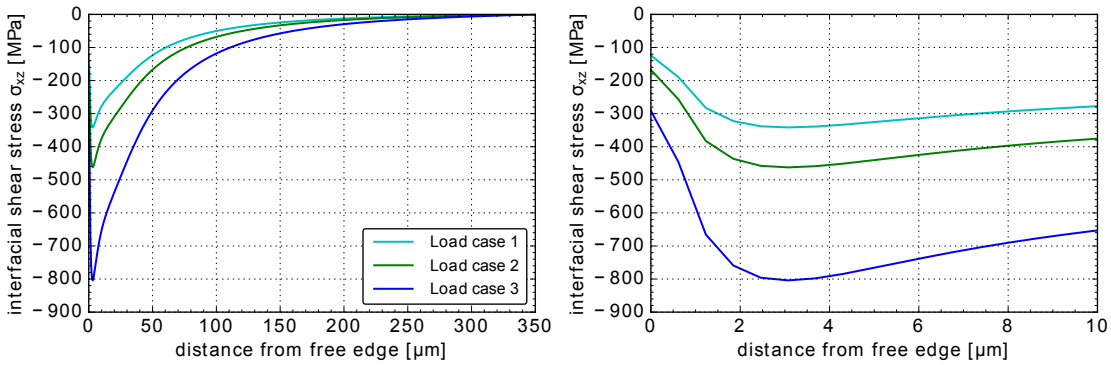


**Figure 4.25:** Interfacial shear stresses for a 1-layer-system subjected to the three load cases (right: detail)

The diagrams show a relatively high value for the shear stress at the free edge which contradicts the requirement that all stress components normal to a free surface must be zero. The reason for this error gets clearer if we review the discussion in [1]. Antretter et al. investigated the effect of free edges at bilayered compounds with an analytical and a numerical model. Both approaches showed an increase of the interfacial shear stress reaching a maximum value very close to the free edge and an immediate drop down to zero in a distance of approximately 1/10000 of the half length of the bilayer. Since the simulation was performed on a bilayer compound with the same thickness for both components, it cannot be compared directly to the configurations considered in the present study. The mesh generating script developed within this framework considers continuum elements for the substrate and shell elements for the individual layers, which makes it difficult to set up models in which both have comparable thickness. However, a comparison of the results shows qualitative similarities. The mesh size considered in the present study is much larger than the mesh required for resolving the stress distribution in the vicinity of the edge where the maximum value drops to zero.

All in all, it can be said, that in order to make a quantitative statement of the stress distribution close to a free edge, further mesh refinement is required.

Further, the interfacial stresses obtained for the reference configuration are investigated. Fig. 4.26 (a)-(c) show the normal and shear stresses in the interface between the substrate and the first layer for the different load cases. It can be observed, that the two individual load cases lead to different shapes of the interfacial stresses.

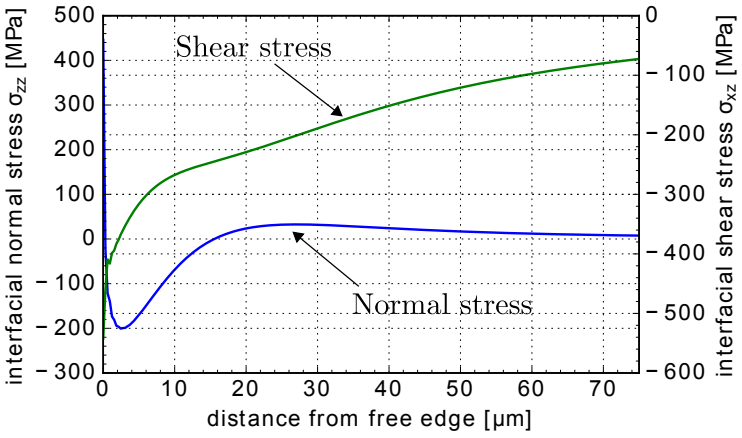


**(a)**

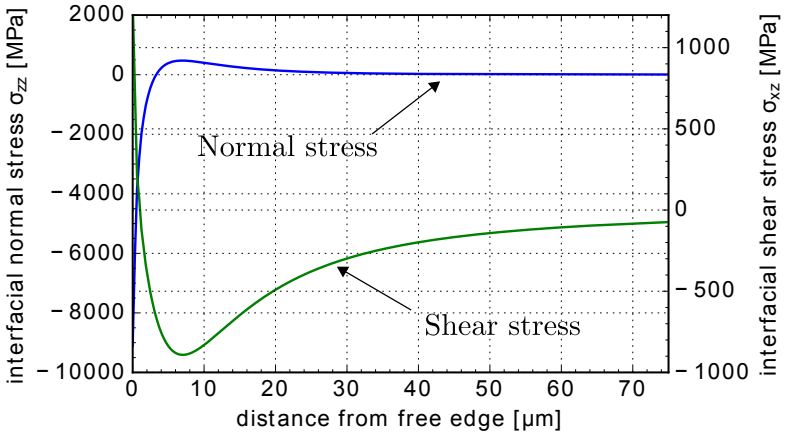


**(b)**

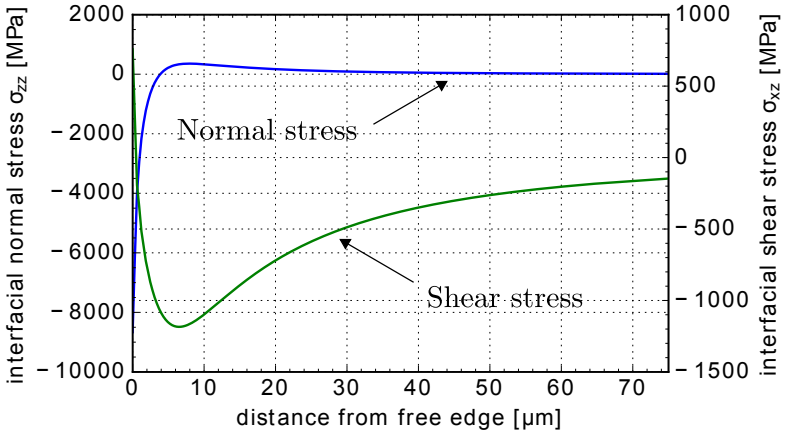


**(c)**

**Figure 4.26:** Interfacial normal and shear stresses obtained for the reference configuration close to the free edge subjected to (a) load case 1 (b) load case 2 (c) load case 3

In order to present the influence of a negative curvature, resulting from changing the substrate material from Austenite to WC-Co, the interfacial normal and shear stress due to thermal loading over the distance form the free surface are plotted in Fig. 4.27. It can be observed that the shear stresses have a similar shape with different signs. The change of the substrate material results in a totally different profile of the interfacial normal stresses.

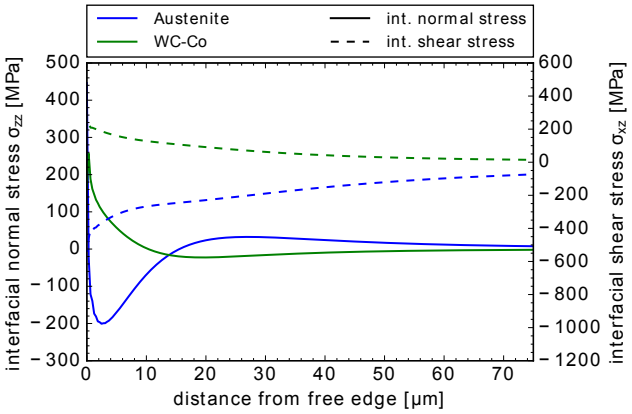


**Figure 4.27:** Interfacial normal and shear stresses between the substrate and the first layer predicted for two different substrate materials and load case 1

As proposed in [9] the stress distribution in an interface of a multilayer coating can be considered as the superposition of the stress profiles schematically illustrated in Fig. 4.28. It shows, that compressive stresses remote from the edge in the upper adjacent component of the considered interface lead to an opening-mode moment, whereas tensile stresses induce a closing moment. According to the contribution of the three stress profiles, the resulting stress distribution can look very differently with more local extrema and different decay lengths. This is not only dependent on the properties/thicknesses of the two adjacent layers, but also on the magnitude and profile of the stress distribution in the entire system. In order to fully understand the influences of the individual parameters, further investigations are required.

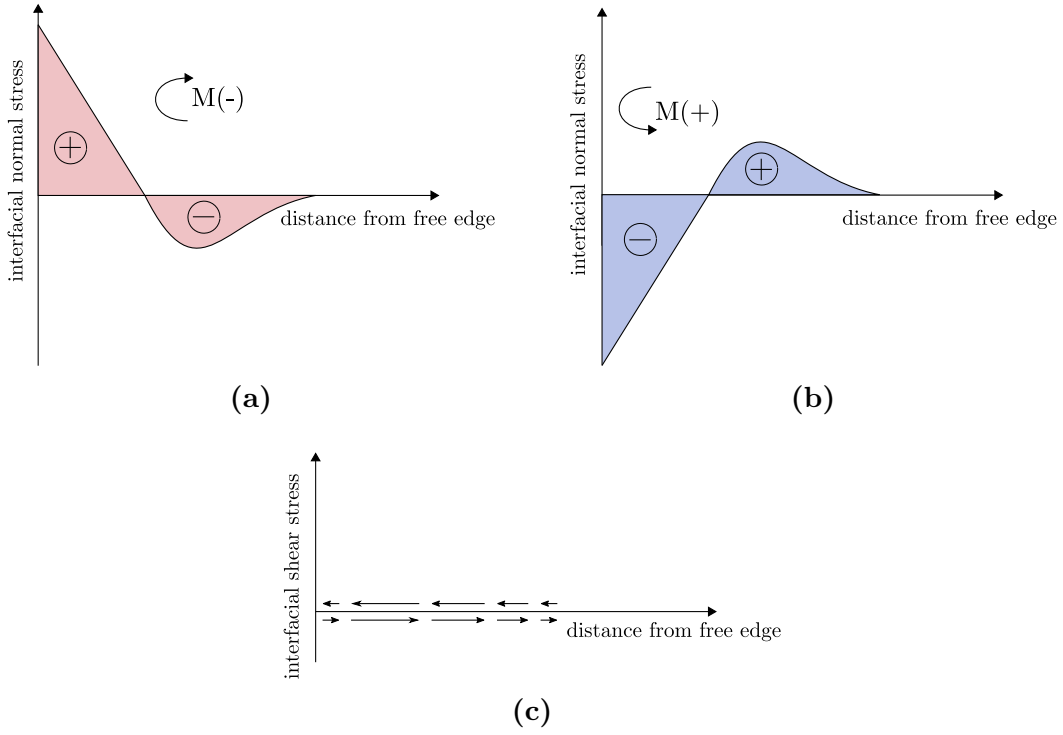


**Figure 4.28:** Schematic illustration of the interfacial stresses.(a) normal stresses with compressive stresses remote from the edge resulting in an opening-mode moment(b) normal stresses with tensile stresses remote from the edge resulting in a closing-mode moment (c) shear stresses being zero at the free edge, increases abruptly and decreases to zero again(modified from [9])

### 4.3.3 Discretization of the semi-infinite plate model

In the following the objective is to discuss the influence of the layer thickness and architecture in a general way, rather than provide quantitative results.

In order to investigate the influence of the layer thickness on the resolution of the interface stresses close to a free edge, a system consisting of a substrate and one single layer is modelled. Three different thicknesses are considered for the layer and a thermal loading of $\Delta T = -480°C$ is applied. The mesh discretization is kept the same for all three cases. In Fig. 4.29(a) the normal interface stress, i.e. the stress parallel to the free surface, is plotted over the distance from the free edge for the interface between the substrate and the coating. A detailed presentation of the area

in the vicinity of the free edge is plotted in Fig. 4.29 (b). What we can learn from this comparison is, that the in the case of a single layer the degree of resolution of the normal stresses in the interface obtained with a certain mesh size is dependent on the thickness of the layer. More precisely, a thinner single-layer coating leads to a worse resolution of the interfacial stresses.

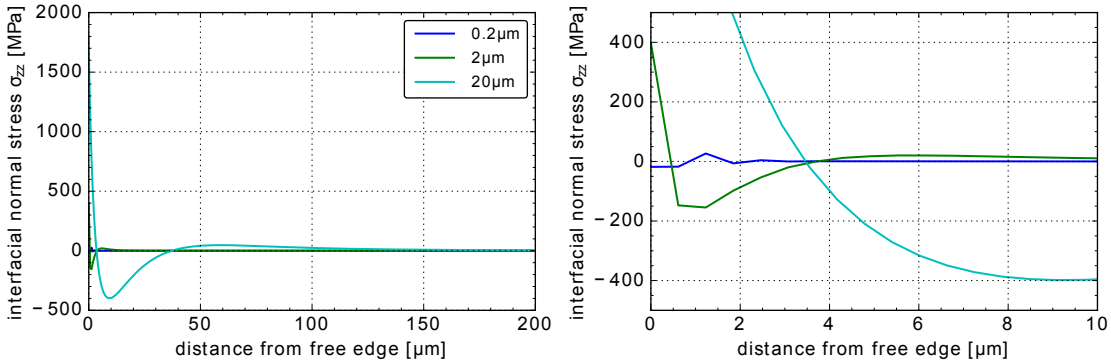


**Figure 4.29:** Influence of the thickness of a single layer coating on the resolution of the interface normal stresses close to a free edge

Since it is aimed to simulate multilayer systems with layers with a thickness of a few nanometers, it is further investigated, whether only the thickness of the adjacent layer defines the required mesh size, or if it is also the total coating thickness. Therefore in a next step a coating thickness of 10$\mu$m is modelled with three different coating architectures. A single layer of TiN, a 40 layer system of TiN (0.2 and 0.3$\mu$m alternately) and a 20 bilayer system of 0.2$\mu$m TiN and 0.3$\mu$m CrN, each being subjected to a thermal loading of $\Delta T = -480°C$, are considered. A comparison of the obtained normal interface stresses of the first interface, i.e. between the substrate and the first layer, is plotted in Fig. 4.30 (a) and (b). Comparing the three different layer architectures, the single layer shows the best resolution in the vicinity of the free edge. Whereas the 40 layers of TiN and the 20 bilayers of TiN/CrN show a comparable resolution. This suggests, that changing the material within a coating does not influence the degree of resolution. However, increasing the number of individual layers within one coating decreases the ability to resolve the distribution of the interfacial stresses. Comparing these results with the resolution of the normal interface stress of

a 0.2$\mu$m thin single layer, Fig. 4.29, one can see, that also the total coating thickness influences the resolution of the interface stresses obtained for a specific mesh size.

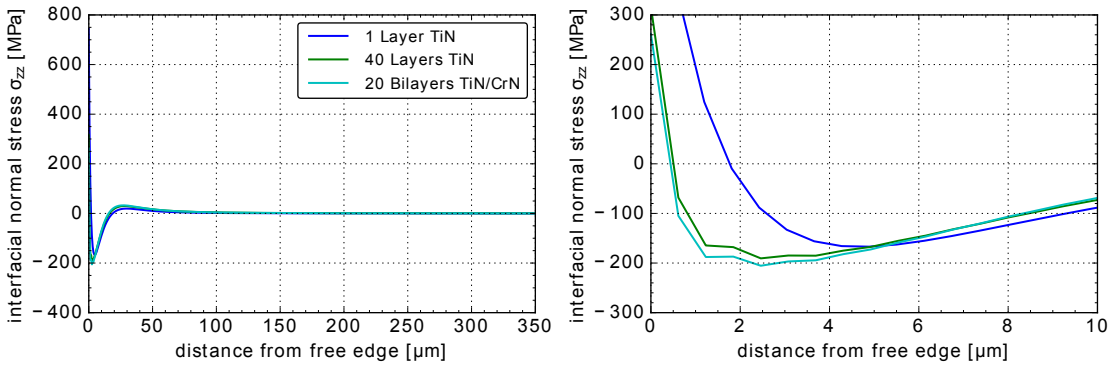


**Figure 4.30:** Influence of the coating architecture on the resolution of the interface normal stresses close to a free edge

Furthermore, the stress distribution in the vicinity of a free edge obtained by two different discretizations is compared. For the fine mesh the elements dimensions normal to the free surface is 0.3$\mu$m, whereas in the coarser mesh it is chosen to be 0.6$\mu$m. A prestress of 3GPa and a thermal loading of $\Delta T = -480°C$ is applied to the reference configuration. The diagrams for the interfacial normal and shear stress indicate, that with both discretizations, the stress distributions are resolved equally well. However, the drop of the interfacial shear stresses to zero cannot be captured with either of the two.

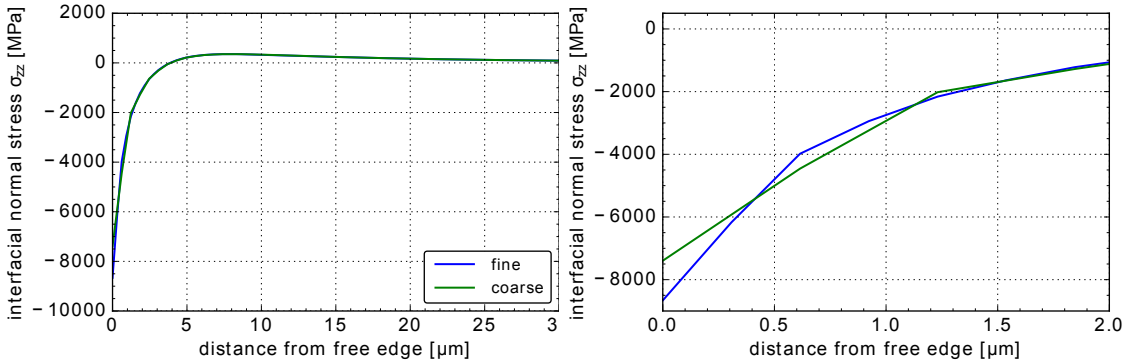


**Figure 4.31:** Influence of the discretization on the interfacial normal stresses close to a free edge (right:detail)

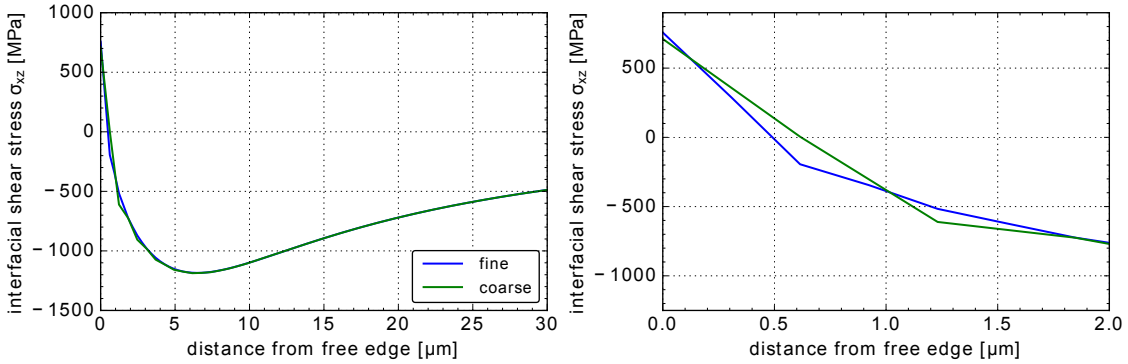


**Figure 4.32:** Influence of the discretization on the interfacial normal stresses close to a free edge (right:detail)

# Chapter 5

# Conclusion

The aim of the present work was to develop an efficient Finite Element model which enables to simulate the residual stress distribution in Multilayer systems. A three dimensional unit cell model with plane periodic boundary conditions was presented. By choosing shell elements for modelling the individual layers and continuum elements for the substrate an efficient model was obtained. The interfaces between the substrate and the layers and between the individual layers was modelled with cohesive elements. Generating the model is parameter controlled and can be easily adjusted to different requirements.

The results obtained for the infinite plate model are in good agreement with analytical solutions. The influence of different parameters on the stress distribution in the system was investigated and qualitative statements concerning the infinite plate model have been made.

By a modification of the boundary conditions a semi-infinite plate model was obtained, which allows capturing free edge effects. The consequences for the stress distribution in the substrate, the coating and the interfaces were investigated. It was found, that the stress profiles at the interfaces depend on various parameters. The presented model can be used to gain deeper insight into the contribution of the individual variables. Furthermore some aspects concerning the mesh discretization close

to a free edge were discussed. In order to provide a quantitative statement about the stress state in the vicinity of a free edge, further mesh refinement is required.
While the presented model provided interesting results concerning the stress distribution in a multilayer system, certain simplifications were made. Within this framework, only isotropic, linear elastic material behaviour was considered in order to test the implemented algorithm. However, the consideration of anisotropic material behaviour and plasticity can be implemented easily in the presented model. One has to keep in mind, that a variation of, e.g., the substrate material often requires an adjustment of different process parameters, which may imply different magnitudes of the applied loading conditions. A variation of the process parameters can further result in a change of the film morphology. This has to be considered when modelling the anisotropic material behaviour.

The model of an infinite plate can further be used to evaluate the influence of a certain void density in the material on its three dimensional stress state.
With the semi-infinite plate model the behaviour in the vicinity of a free edge can be further investigated and the delamination process can be considered.

# Appendix A

# Procedure to generate a sample

Fig. A.1 shows a schematic illustration of the necessary steps to generate the master input file for an FE-simulation of a multilayer system.

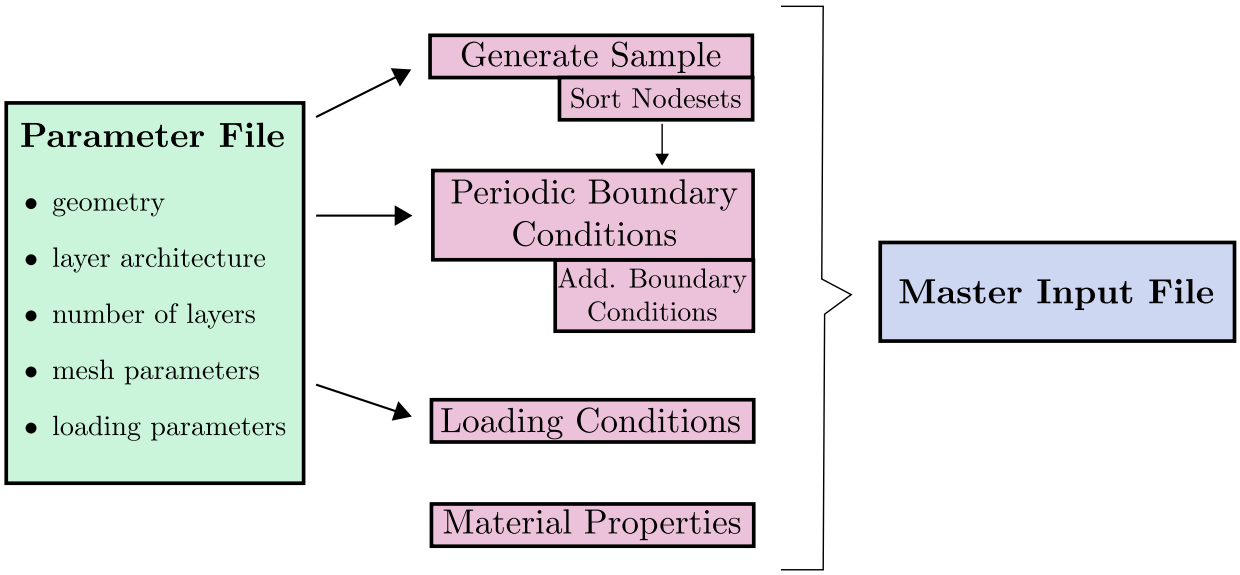


**Figure A.1:** Procedure to generate the master input file

# Appendix B

# Contour plots of the semi-infinite plate model

Fig. B.2 and Fig. B.1 show the contour plots of the substrate and the coating, respectively, obtained from the FE-simulation of the semi-infinite model for the reference configuration. For a better clearness only the region in the vicinity of the free edge is plotted with the free surface being on the right side.

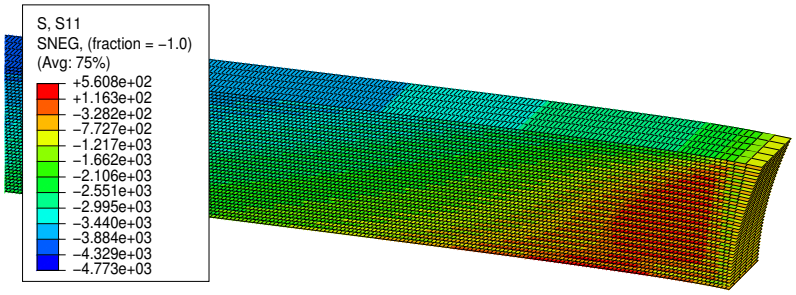


**(a)**

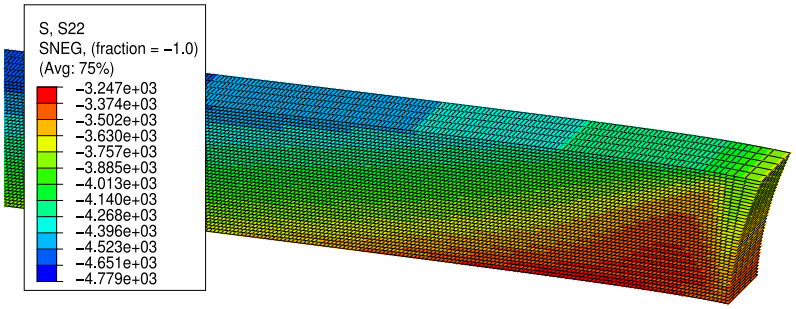


**(b)**

**Figure B.1:** Influence of a free edge on the total residual stress distribution in the coating (a) in-plane stress normal to the free surface (b) in-plane stress parallel to the free surface

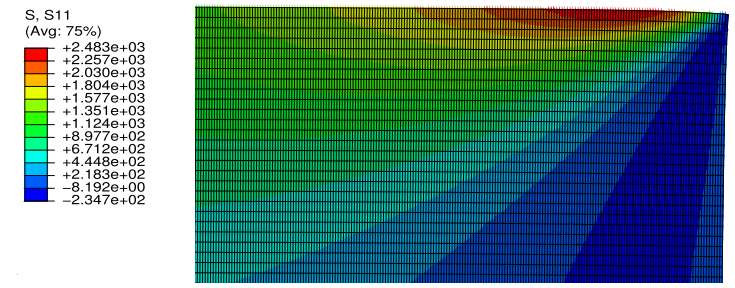


**(a)**

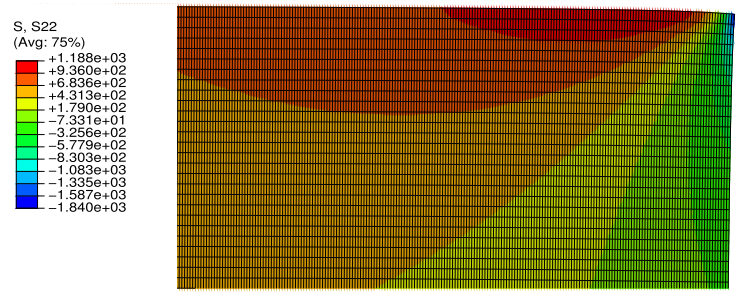


**(b)**

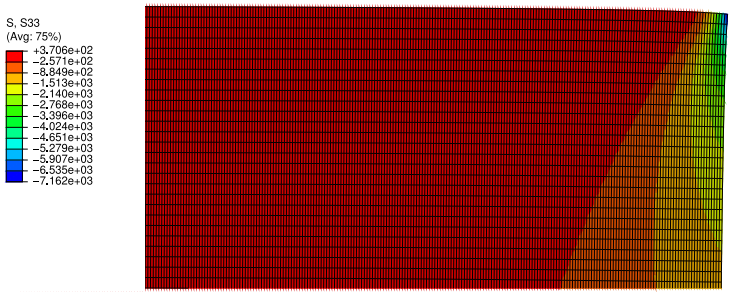


**(c)**

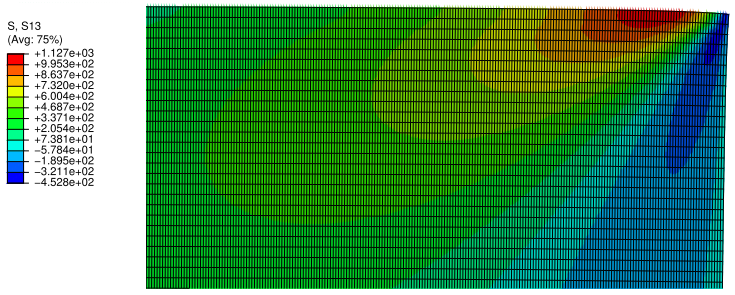


**(d)**

**Figure B.2:** Influence of a free edge on the total residual stress distribution in the substrate (a) in-plane stress normal to the free surface (b) in-plane stress parallel to the free surface (c) out-of plane normal stress (d) out-of plane shear stress

# Bibliography

[1] T. Antretter, F. D. Fischer, F. G. Rammerstorfer, and Zickler G. A. Free edges at bilayered compounds - a short analytical and numerical consideration. *Archive of applied mechanics*, 86:2053–2061, 2016.

[2] D. S. Balint and J. W. Hutchinson. Mode II edge delamination of compressed films. *Journal of Applied Mechanics*, 68:725–730, 2001.

[3] R. F. Bunshah. *Handbook of Deposition Technologies for Films and Coatings*. Noyes Publications, 1994.

[4] T. Ceglar. *Finite element method simulations of the delamination in laminated composite structures*. Master's thesis, Institute of Lightweight Design and Structural Biomechanics, Vienna University of Technnology, 2016.

[5] E. Chason and P. R. Guduru. Tutorial: Understanding residual stress in polycrystalline thin films through real-time measurements and physical models. *Journal of Applied Physics*, 119:191101–1–191101–21, 2016.

[6] L. B. Freund and S. Suresh. *Thin film materials: Stress, Defect Formation and Surface Evolution*. Cambridge, 2009.

[7] R. Hahn, M. Bartosik, R. Soler, C. Kirchlechner, G. Dehm, and P.H. Mayrhofer. Superlattice effect for enhanced fracture toughness of hard coatings. *Scripta Materialia*, 124:67–70, 2016.

[8] P. W. Harper and R. Hallett. Cohesive zone length in numerical simulations of composite delamination. *Engineering Fracture Mechanics*, 75:4774–4792, 2008.

[9] C. H. Hsueh and C. R. Luttrell. Interfacial peeling moments and shear forces at free edges of multilayers subjected to thermal stress. *Journal of the American Ceramic Society*, 89:1632–1638, 2006.

[10] J. W. Hutchinson. Stresses and failure modes in thin films and multilayers. *Notes for a DCAMM course*, 1996.

[11] R. N. Ibrahim, M. A. Rahmat, R. H. Oskouei, and R. K. Singh Raman. Monolayer TiAlN and multilayer TiAlN/CrN PVD coatings as surface modifiers to migitate fretting fatigue of AISI P20 steel. *Engineering Fracture Mechanics*, 137:64–78, 2015.

[12] G. C. A. M. Janssen. Stress and strain in polycrystalline thin films. *Thin Solid Films*, 515:6654–6664, 2007.

[13] G. Kienel. *Vakuumbeschichtung 4.* VDI Verlag, 1993.

[14] A. Li, J. Zhao, J. Zang, and Zheng W. Design and simulation of thermal residual stresses of coatings on WC-Co cemented carbide cutting tool substrate. *Journal of Mechanical Science and Technology*, 30:3777–3783, 2016.

[15] B. Li. 3D FEM modelling for stress simulation and experimental investigation of dual-gradient coating using PVD. *International Journal of Materials Research*, 107:300–308, 2016.

[16] S. Massl, Keckes J., and Pippan R. A direct method of determining complex depth profiles of residual stresses in thin films on a nanoscale. *Acta Materialia*, 55:4835–4844, 2007.

[17] D. M. Mattox. *Handbook of Physical Vapor Deposition Processes.* Elsevier, 2010.

[18] P. H. Mayrhofer. *Surface Technology.* Institute of Materials Sience and Technology, 2015.

[19] R. Messier, A.P. Giri, and R.A. Roy. Revised structure zone model for thin film physical structure. *Journal of Vacuum Science and Technology*, A 2:500, 1984.

[20] M. Nagler. Analytical treatment of residual stresses in multilayer coatings. Master's thesis, Institute of Lightweight Design and Structural Biomechanics, Vienna University of Technnology, 2017.

[21] H. Oettel and R. Wiedemann. Residual stresses in PVD hard coatings. *Surface and Coatings Technology*, 76-77:265–273, 1995.

[22] D. H. Pahr. Linear and non-linear homogenization using fem. *ILSB-Report*, 2004.

[23] R. Schoengrundner, R. Treml, T. Antretter, D. Kozic, W. Ecker, D. Kiener, and R. Brunner. Critical assessment of the determination of residual stress profiles in thin films by means of the ion beam layer removal method. *Thin Solid Films*, 564:321–330, 2014.

[24] F. Spaepen. Interfaces and stresses in thin films. *Acta Materialia*, 48:31–42, 2000.

[25] G. G. Stoney. The tension of metallic films deposited by electrolysis. *Proceedings of the Royal Society of London*, 82:172–175, 1909.

[26] M. Stueber, H. Holleck, H. Leiste, K. Seemann, S. Ulrich, and C. Ziebert. Concepts for the design of advanced nanoscale PVD multilayer protective thin films. *Journal of Alloys and Compounds*, 483:321–333, 2009.

[27] Dassault Systems Simulia Corp. *Abaqus/Standard User's Manual*, Version 6.14. Providence, RI, USA.

[28] V. Teixeira. Residual stress and cracking in thin PVD coatings. *Vacuum*, 64: 393–399, 2002.

[29] J. A. Thornton. Influence of apparatus geometry and deposition conditions on the structure and topography of thick sputtered coatings. *Journal of Vacuum Science and Technology*, 11:666–670, 1974.

[30] Y. C. Tsui and T. W. Clyne. An analytical model for predicting residual stresses in progressively deposited coatings. *Thin Solid Films*, 306:23–33, 1997.

[31] E. Vogli, W. Tillmann, U. Selvadurai-Lassl, G. Fischer, and J. Herper. Influence of Ti/TiAlN-multilayer designs on their residual stresses and mechanical properties. *Applied Surface Science*, 257:8550–8557, 2011.

[32] U. Wiklund, J. Gunnars, and S. Hogmark. Influence of residual stresses on fracture and delamination of thin hard coatings. *Wear*, 232:262–269, 1999.

[33] H. H. Yu, M. Y. He, and J. W. Hutchinson. Edge effects in thin film delamination. *Acta Materialia*, 49:93–107, 2001.

[34] J. Zhu, Xie H., Z. Hu, P. Chen, and Q. Zhang. Residual stress in thermal spray coatings measured by curvature based on 3D digital image correlation technique. *Surface and Coatings Technology*, 206:1396–1402, 2011.